OXFORD

REVIEW

Fundamental functional differences between gyri and sulci: implications for brain function, cognition, and behavior

Xi Jiang[1,#], Tuo Zhang[2,#], Shu Zhang[3], Keith M. Kendrick[1] and Tianming Liu[4,*]

[1]School of Life Science and Technology, MOE Key Laboratory for Neuroinformation, University of Electronic Science and Technology of China, Chengdu 611731, China
[2]School of Automation, Northwestern Polytechnical University, Xi'an 710129, China
[3]Center for Brain and Brain-Inspired Computing Research, School of Computer Science, Northwestern Polytechnical University, Xi'an 710129, China
[4]Cortical Architecture Imaging and Discovery Laboratory, Department of Computer Science and Bioimaging Research Center, The University of Georgia, Athens, GA 30605, USA

*Correspondence: Tianming Liu, tliu@cs.uga.edu
#Co-first authors.

Abstract

Folding of the cerebral cortex is a prominent characteristic of mammalian brains. Alterations or deficits in cortical folding are strongly correlated with abnormal brain function, cognition, and behavior. Therefore, a precise mapping between the anatomy and function of the brain is critical to our understanding of the mechanisms of brain structural architecture in both health and diseases. Gyri and sulci, the standard nomenclature for cortical anatomy, serve as building blocks to make up complex folding patterns, providing a window to decipher cortical anatomy and its relation with brain functions. Huge efforts have been devoted to this research topic from a variety of disciplines including genetics, cell biology, anatomy, neuroimaging, and neurology, as well as involving computational approaches based on machine learning and artificial intelligence algorithms. However, despite increasing progress, our understanding of the functional anatomy of gyro-sulcal patterns is still in its infancy. In this review, we present the current state of this field and provide our perspectives of the methodologies and conclusions concerning functional differentiation between gyri and sulci, as well as the supporting information from genetic, cell biology, and brain structure research. In particular, we will further present a proposed framework for attempting to interpret the dynamic mechanisms of the functional interplay between gyri and sulci. Hopefully, this review will provide a comprehensive summary of anatomo-functional relationships in the

cortical gyro-sulcal system together with a consideration of how these contribute to brain function, cognition, and behavior, as well as to mental disorders.

Key words: cortical folding; gyro-sulcal pattern; brain anatomo-function

Introduction

Cortical folding is a hallmark of brain topography whose variability across individuals and groups is strongly coupled with inter-individual and inter-group differences in brain function, cognition, and behavior. Gyri and sulci are the standard nomenclature (Fig. 1) and are usually defined and applied to anatomical domains (Cachia et al., 2003a; Toro and Burnod, 2003). The anatomical and functional relationships between gyri and sulci have not been clearly elucidated. For example, at a coarser resolution of cortical region parcellation, primary sulci have relatively more constant relationships with cytoarchitecture or functional architecture, while the accuracy of this alignment drops for secondary/tertiary sulci on higher-order association cortices involved in complex cognitive functions (Zilles et al., 1997; Roland and Zilles, 1998; Hasnain et al., 2001; Morosan et al., 2001; Fischl et al., 2008; Hinds et al., 2008; Frost and Goebel, 2012). An increasing number of studies over the last decade have therefore investigated, at a finer resolution, whether these two elementary anatomical units could serve as building blocks of cortical morphology and brain function, and whether they could be functionally and cognitively differentiated (e.g. Uddin et al., 2010; Deng et al., 2014; Jiang et al., 2015a, 2018a).

It has been demonstrated repeatedly that the local gyro-sulcal morphology of many cortical regions could predict the location of functional activity in adult human brains (Amiez et al., 2006, 2013; Benson et al., 2012; Amiez and Petrides, 2014, 2018; Li et al., 2015; Weiner et al., 2018; Troiani et al., 2020). For instance, the locations of visuomotor eye and hand conditional activity are localized in different sub-regions within the superior precentral sulcus (Amiez et al., 2006). The retinotopic organization of striate cortex can be predicted by surface topology (Benson et al., 2012) and feedback-related activity during exploration is differentially located in the cingulate sulcus and paracingulate sulcus of different individuals (Amiez et al., 2013). There are also three somatotopically organized cingulate motor areas along the cingulate sulcus, each of which is associated with specific morphological features of the cingulate/paracingulate cortex (Amiez and Petrides, 2014). The functional activities of different action controls are localized in different sulci in the posterior lateral frontal cortex (Amiez and Petrides, 2018) and different value signals are localized in different sulcal regions of the orbitofrontal cortex (Li et al., 2015; Troiani et al., 2020). Moreover, local gyro-sulcal morphology can predict the location of functional organization in adult human brains, with the presence/absence of the inferior rostral sulcus and the subgenual intralimbic sulcus influencing inter-participant variability in the ventromedial prefrontal cortex (vmPFC) sulcal morphology, and the vmPFC peak location in the default mode network (Lopez-Persem et al., 2019).

Associations between gyro-sulcal patterns and human behavior have also been demonstrated to investigate brain-behavior relationships as well as neuropsychological correlates of inter-participant cortical folding variations (Fornito et al., 2004; Whittle et al., 2009; Cachia et al., 2018; Yang et al., 2019). For instance, inter-participant differences in paracingulate sulcus asymmetry in healthy males have been shown to be related to individual differences in executive abilities in cognitively demanding tasks (Fornito et al., 2004). The leftward anterior cingulate cortex asymmetry pattern of male early adolescents is associated with individual differences in temperament (Whittle et al., 2009). Adults whose left lateral occipito-temporal sulcus were interrupted by the gyrus in the posterior portion showed better reading fluency than those who had a continuous one, and the greater the interruption, the better was their performance (Cachia et al., 2018). Another study reported more gyral than sulcal regions within the middle frontal cortex, inferior parietal lobe, and visual cortex, for which rs-fMRI signal temporal variability was positively correlated with fluid intelligence (Yang et al., 2019). In addition to studies on adults, one on newborns has reported that there were specific morphological characteristic differences between twins and singletons, as well as between normally developed newborns and those with intrauterine growth restriction. Indeed, these brain morphological measures at birth could predict infants' cerebral volumes and neurobehavioral development at term-equivalent age (Dubois et al., 2008).

To measure brain functional activity, functional magnetic resonance imaging (fMRI), rather than other techniques including electroencephalography (EEG), magnetoencephalography (MEG), and functional near infrared spectroscopy (fNIRS), has been predominantly adopted for gyro-sulcal functional characteristic studies. This has been due to the development of advanced in vivo fMRI technologies for both high spatial and temporal resolution that can both guarantee accuracy of gyri/sulci localization and measure the bandwidth range of their blood oxygen level dependent (BOLD) signals (Biswal et al., 1995; Logothetis, 2008; Friston, 2009; Van Essen et al., 2013). Gyro-sulcal functional characteristics have been extensively studied during performance of different tasks based on task-based fMRI (t-fMRI) (Logothetis, 2008; Friston, 2009; Barch et al., 2013), or during task-free rest conditions based on resting state fMRI (rs-fMRI) (Biswal et al., 1995; Smith et al., 2013). In addition to the commonly adopted fMRI data in volume space, the Human Connectome Project (HCP) has also publicly released "grayordinate" fMRI data (Barch et al., 2013; Glasser et al., 2013;
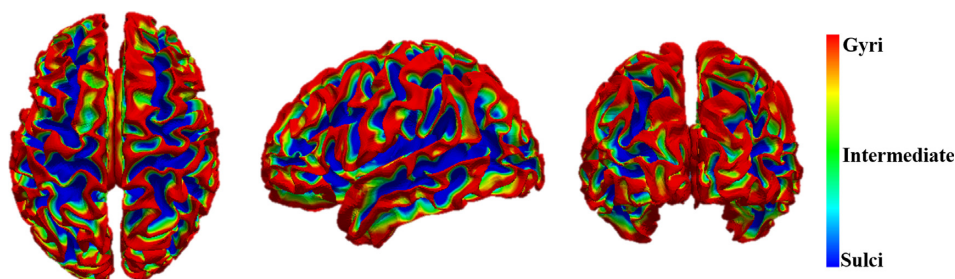
Figure 1: The gyral/sulcal parcellation of cortical surface based on the anatomical information (average convexity in this figure, adapted from Liu *et al.*, 2019). Gyri has larger average convexity than sulci.

Smith *et al.*, 2013; Van Essen *et al.*, 2013). The HCP grayordinate data consists of both cortical surface vertices and subcortical voxels of gray matter in the standard MNI152 space, which correspond closely across different individual brains to facilitate group-wise analysis (Glasser *et al.*, 2013). The grayordinate fMRI (including both t-fMRI and rs-fMRI) data is especially suitable for gyro-sulcal functional characteristic studies since the gyri/sulci as well as their fMRI signals are defined on the cortical surface vertices with satisfying accuracy in the grayordinate space (Glasser *et al.*, 2013). In this review, our focus will be on fMRI-based studies since reported findings are substantially more extensive and better established.

This review article will include the following sections: (i) a review of gyral/sulcal definition and labeling scheme in individual brains; (ii) a review of structural substrates for gyro-sulcal functional differences; (iii) a review of the major findings of gyro-sulcal functional differences; (iv) a dynamic functional model of gyri and sulci; and (v) discussion of future research priorities.

Gyral/Sulcal Definition and Labeling Scheme in Individual Brains
Definition of gyri and sulci

In previous studies, gyri and sulci are usually treated as morphological and anatomical nomenclature, and usually defined based on morphological features (Li G. *et al.*, 2009, 2010). For example, in FreeSurfer (Fischl, 2012), a mid-surface is defined such that the displacements of all vertices from their original locations to it are summed to zero. Usually, gyral vertices have negative values (larger average convexity) and sulcal vertices have positive values (Fig. 1). An alternative approach is labeling sulci and gyri via matching individual images to a gyro-sulcal atlas. This approach has caught the attention of neuroscientists since the pioneering work of Brodmann (1909), which demonstrates that architectonic/functional boundaries align with sulci on human brains (Watson *et al.*, 1993; Roland and Zilles, 1994; Tzourio-Mazoyer *et al.*, 2002; Fischl *et al.*, 2008). Although this anatomy–function relation is less pronounced in secondary and tertiary cortices across participants due to great inter-individual variabilities in folding geometry (Fischl *et al.*, 2008; Ono *et al.*, 1990), major sulci and gyri, which develop earlier, have usually been used as anatomical proxies, or

landmarks, to align macroscale functional regions. It is worth noting that biological definition and delineation of gyral and sulcal regions, as well as the transition area of gyral wall, warrants extensive studies in the future.

Methods for sulci/gyri labeling

In general, there are two main methods for sulci/gyri labeling. The first method uses deformable registration to warp the labeled sulci/gyri on template to a single subject (Behnke *et al.*, 2003; Desikan *et al.*, 2006). Most of these registration methods were traditionally designed to achieve automatic volumetric alignment but do not constrain cortices to align (Talairach and Szikla, 1967; Woods *et al.*, 1998; Johnson and Christensen, 2002; Shen and Davatzikos, 2003; Joshi *et al.*, 2007). With an increasing interest in cortex, many recent registration approaches have been performed on the entire cortical surface, rather than volumes, to align shape metrics such as curvature and sulcal depth (Fischl *et al.*, 1999; Tosun, Rettmann and Prince, 2004; Goebel *et al.*, 2006). These methods, aiming at the alignment of the entire volume or cortical surface, however, could lead to misalignment of cortical landmarks of interest such as sulci/gyri (Pantazis *et al.*, 2010). Therefore, in a second method, manually or automatically identified landmarks, such as sulci/gyri, have been explicitly used to constrain the registrations of volumes and surfaces (Thompson and Toga, 1996; Davatzikos, 1997; Joshi and Miller, 1997; Collins *et al.*, 1998; Van Essen *et al.*, 1998; Thompson *et al.*, 2000; Hellier and Barillot, 2003; Glaunes *et al.*, 2004; Van Essen, 2005; Desikan *et al.*, 2006; Joshi *et al.*, 2007). These methods have thus demonstrated achievement of direct improvement of the cross-subject correspondence for landmarks (Desai *et al.*, 2005; Pantazis *et al.*, 2010).

In addition to the registration methods, there are studies that directly identify and label sulci/gyri in individual spaces from volumes and cortical surfaces (Mangin *et al.*, 1995; Goualher *et al.*, 1997; Lohmann, 1998; Lohmann and von Cramon, 2000; Zhou *et al.*, 1999; Rivière *et al.*, 2002; Rettmann *et al.*, 2002; Kao *et al.*, 2007; Li G *et al.*, 2009, 2010). These methods preserve inter-individual variability to the best extent, especially for the secondary and tertiary sulci/gyri, but still might need additional steps (possibly registration methods) before or after the labeling in individual space to estimate cross-subject correspondence (Joshi *et al.*, 2012).

In summary, these sulci/gyri labeling methods were developed on a prerequisite that these anatomic landmarks align well with brain cytoarchitecture and functions such that they can be used as a proxy. However, such a relationship is variable in more developed higher-order cortices (Ono *et al.*, 1990; Cachia *et al.*, 2003b; Fischl *et al.*, 2008), which have abundantly more variable secondary and tertiary cortical folding that could often produce misalignment across participants or unsatisfactory labeling in individual spaces. Therefore, a fundamental improvement could possibly be achieved by exploring a more precise and higher-resolution mapping between folding patterns and brain cytoarchitecture or brain functions.

Structural Substrates for Gyro-Sulcal Functional Differentiation

Neuronal processes and gyro-sulcal pattern development

The developing brain undergoes a number of complicated and inter-related neuronal processes (Smart *et al.*, 2002; Betizeau *et al*, 2013; Borrell and Götz, 2014; Florio and Huttner, 2014; Lewitus *et al*, 2014; Taverna *et al.*, 2014). Many of these processes have been demonstrated to be relevant to cortical folding and even to specific gyral/sulcal patterns (Noctor *et al.*, 2004; Englund *et al.*, 2005; Fietz *et al.*, 2010; Hansen *et al.*, 2010; Reillo *et al.*, 2011; Wang *et al.*, 2011; Reillo and Borrell, 2012; Betizeau *et al.*, 2013; Pilz *et al.*, 2013; de Juan Romero and Borrell, 2015; Johnson *et al.*, 2015). In particular, the abundance of basal radial glia cells (bRGCs) in the outer subventricular zone (oSVZ) is suggested to be tangentially heterogeneous (Borrell and Gotz, 2014), such that an increase in bRGC number in local areas gives rise to the fanning-out of a radial fiber scaffold and dispersion of radially migrating neurons, leading to a gyrus-like structure in the corresponding locations in the cortical plate while the germinal layers remain unfolded (Fietz *et al.*, 2010; Hansen *et al.*, 2010; Reillo *et al.*, 2011; Wang *et al.*, 2011; Pilz *et al.*, 2013; Stahl *et al.*, 2013; Borrell and Götz, 2014; Gertz and Kriegstein, 2015). The regulation of basal progenitor heterogeneity in the fetal phase persists in the mature stage. Gyri also have a relatively higher absolute cortical thickness and total neuron number, especially in the deep cortical layers (V + VI) (Hiletag and Barbas, 2005).

However, it is still unclear whether the timing of abundance of progenitors in oSVZ is concordant with that of gyrogenesis (Kroenke and Bayly, 2018), because the cerebrum is still lissencephalic when neurogenesis is complete around embryonic day (E) 90 (Rash *et al.*, 2019). In this regard, other processes, such as gliogenesis, axonogenesis, and myelinogenesis are also correlated with the development and growth of cortical folding (Chi *et al.*, 1977; Huang *et al.*, 2009; Takahashi *et al.*, 2010, 2012; White *et al.*, 2010; Dubois *et al.*, 2014; Hagemeyer *et al.*, 2017; Rash *et al.*, 2019). Taking gliogenesis as an example, as the oSVZ grows, more astrocytes and oligodendrocytes are produced than neurons until after E125, which coincides with the formation of white matter cortical connections and the onset of gyrification (∼E100–E125). Nevertheless, the contribution of gliogenesis alone may be insufficient to induce cortical folding and may additionally need to be considered jointly considered with axonogenesis (Rash *et al.*, 2019). Axonogenesis has been relatively better studied and is more closely related to cortical folding, not only due to its concomitant occurrence with gyrification (Huang *et al.*, 2009; White *et al.*, 2010; Takahashi *et al.*, 2012; Dubois *et al.*, 2014), but also due to abundant direct support from observations that manipulations of axon growth lead to massive alterations in gyrification patterns (Rakic, 1988).

Neuronal processes and gyro-sulcal functional differentiation

The heterogeneity in neuron distribution (Hiletag and Barbas, 2005) and axon distribution (Huang *et al.*, 2009; Takahashi *et al.*, 2012; Ouyang *et al.*, 2017), induced by the processes described in the section of 'Neuronal processes and gyro-sulcal pattern development', is related to gyro-sulcal functional differentiation. Within the cortex, somata and arbors of pyramidal neurons are stretched in gyri and compressed in sulci due to the heterogeneity in neuron numbers (Hiletag and Barbas, 2005), resulting in different lengths of apical segments. Identical neurons with different lengths of apical segments have been demonstrated to produce different types of action potentials (Fig. 2A, Hiletag and Barbas, 2005). Thus, differences in dendrite morphology between sulci and gyri result in putative functional differences in attenuation of excitatory postsynaptic potentials, and possibly provide a fundamental explanation for gyro-sulcal differences in fMRI signal time-frequency characteristics outlined in the section of 'Gyro-sulcal functional activity time-frequency differences'.

Axonal transmission of action potentials is a key component of communication between neurons and a variety of theories have been proposed to interpret the contribution of axons to gyro-sulcal patterns and their related functional architecture (Van Essen, 1997; Xu *et al.*, 2010; Nie *et al.*, 2012; Budde and Annese, 2013; Chen *et al.*, 2013; Zhang *et al.*, 2014). In Van Essen, 1997, axons were found to be under a form of tension and assumed to pull cortical regions closer to each other. The cortical regions being pulled became gyral walls or sulci, leaving the other interleaved cortical regions with weaker axonal connections as gyri. Although tension along axons has been demonstrated by microdissection, the axons, as shown in Fig. 2B, were aligned circumferentially beneath the sulcal depth and radially inside gyri (Xu *et al.*, 2010). Such a spatial relation between axons and gyro-sulcal patterns, which has gained support from both microscale (Budde and Annese, 2013) and macroscale observations (Nie *et al.*, 2012; Zhang *et al.*, 2014), is, however, not consistent with the proposed caudal effects of axon tension on folding in Van Essen(1997). Despite the spatial relation argument, there might nevertheless be a consensus that axonal wiring patterns are different between gyri and
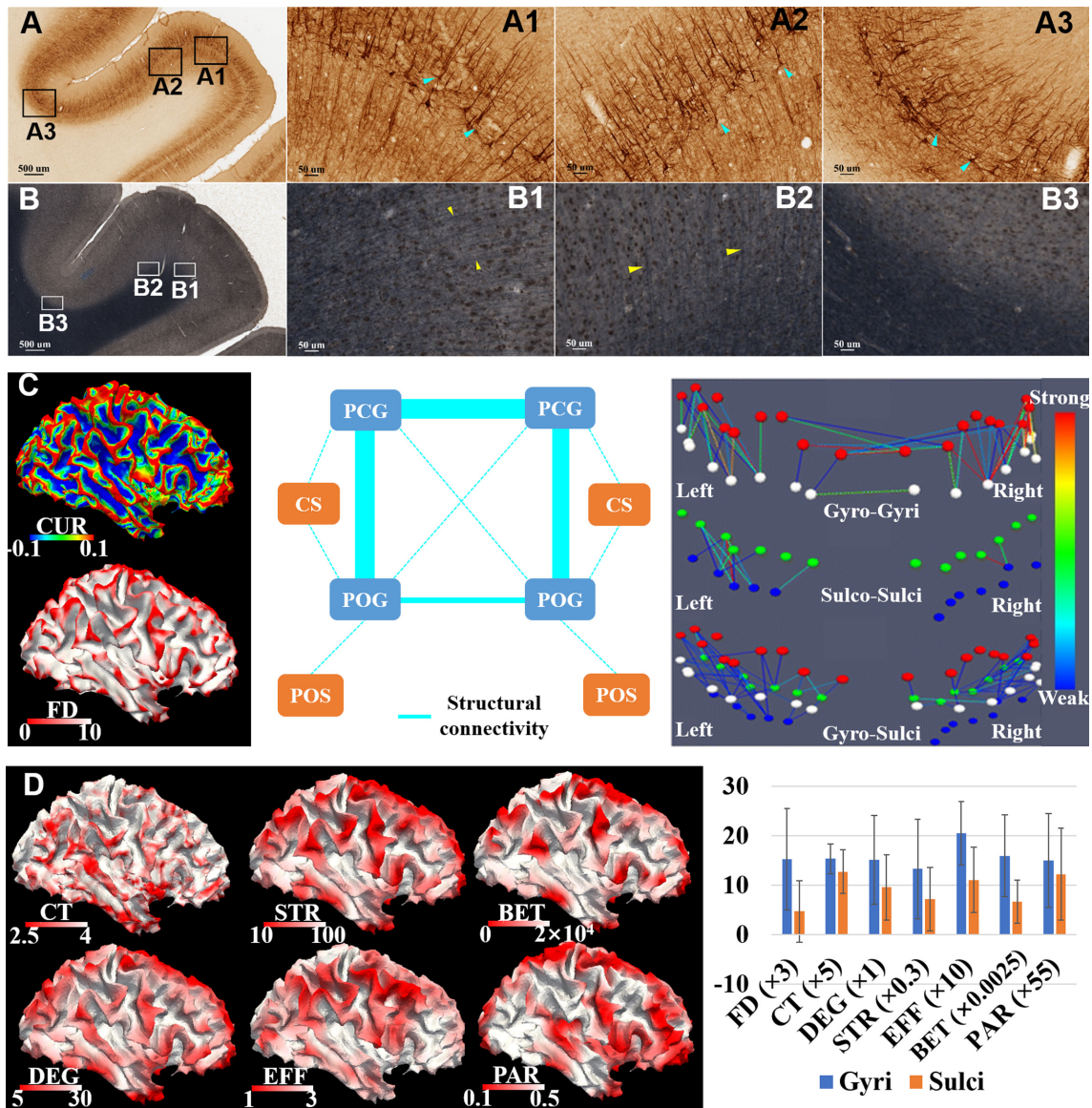
Figure 2: (**A**) A low magnification overview of coronal sections through 8AD (area 8 of cortex, anterodorsal part) and 8B (area 8B of cortex) in the rhesus monkey prefrontal cortex. Tissue was processed for SMI-32, which labels largely pyramidal neurons in cortical layers II + III and V + VI. (A1)–(A3) High magnification views of layer V and II at the gyral crest and gyral wall in 8AD, and sulcal fundus in 8B. Arrowheads highlight the neurons of typical morphologies. Elongated dendritic arbors and cell bodies are observed in (A1) and (A2) while tangentially oriented dendrites and flattened cell bodies are observed in (A3). (**B**) A low magnification overview of coronal section through 8AD and 8B. Weil's stain was applied to the tissue, where the myelin sheaths are stained dark blue. (B1)–(B3) High magnification views of boundaries between white matters and gray matters at gyral crest and gyral wall in 8AD, and sulcal fundus in 8B. Arrowheads in (B1) and (B2) highlight the myelin sheaths that radially oriented across the boundaries. Such myelin sheaths are barely seen in (B3), where myelin sheaths tangentially course along the sulcal fundus. These data in (A) and (B) were available at http://brainmaps.org (Mikula *et al.*, 2007). (**C**) White matter axonal wiring patterns between gyri and sulci. Left column: maximum principal curvature (CUR) and diffusion tensor imaging (DTI) derived white matter fiber density (FD) were mapped to the cortical surface as references. Middle: illustration of DTI fiber connection strength between precentral gyri (PCG, postcentral gyri (POG), central sulcus (CS), and postcentral sulcus (POS) on two hemispheres. Line thickness indicates the connection strength. Right: DTI fiber connections between PCG, POC, CS, and POS in detail. The red, white, green, and blue bubbles represent the regions of interest (ROI) on PCG, POG, CS, and POS, respectively. Lines between ROI as well as the colors indicate the presence of connections and their strength. These figures in the middle and the right panels were adapted from Deng *et al.*, 2014. (**D**) Left: cortical thickness (CT) and graphic metrics, including the degree (DEG), strength (STR), efficiency (EFF), betweenness (BET), and participation (PAR) of a structural connective network mapped to a white matter cortical surface. Right: comparison between gyri and sulci regarding the metrics in (C) and (D). These figures are adapted from Zhang *et al.*, 2020.

sulci. Also, axonogenesis is unlikely to be the only driving force for cortical folding since other neuronal maturation and mechanical processes could make significant contributions (Bayly *et al.*, 2013; Ronan *et al.*, 2014; Razavi *et al.*, 2015; Zhang *et al.*, 2016, 2017).

More importantly, the different axonal wiring patterns between gyri and sulci suggest that they may play different functional roles (Van Essen, 1997; Deng *et al.*, 2014; Zhang *et al.*, 2020). According to parsimonious principles of brain development (Chklovskii *et al.*, 2002;

Laughlin and Sejnowski, 2003; Bullmore and Sporns, 2012), Van Essen (1997) has proposed that cortical regions connected by denser axons are pulled closer to each other, such that the information communication and wiring construction costs are reduced. However, the cortico-cortical axon wiring diagram in this theory seems to consist of repeated units: cortical pairs connected by axons. If the axon-tension solution for wiring optimization is applied to all units, however, there would only be short-range connections over the entire cortex. In fact, many studies have reported the presence of considerable number of long-range axons, and that the nature of the axon wiring diagram is a "small-world" or "rich-world" network rather than a composition of repeated units linked by local short-range axons (Watts and Strogatz, 1998; He *et al.*, 2007; van den Heuvel and Sporns, 2011; van den Heuvel *et al.*, 2012). Brain networks allow the presence of long-range connections between gyri (Xu *et al.*, 2010; Nie *et al.*, 2012; Budde and Annese, 2013; Chen *et al.*, 2013; Deng *et al.*, 2014; Zhang *et al.*, 2014), which are distant from one other. Regarding cortical folding patterns, long-range gyro-gyral white matter connections have been demonstrated to be stronger than gyro-sulcal and sulco-sulcal ones (Fig. 2C, Nie *et al.*, 2012; Deng *et al.*, 2014). These long-range gyro-gyral connections introduce a higher wiring cost but this can be offset by their higher capacity as shortcuts in reducing communication steps and upgrading global integration in brain networks (Kaise and Hilgetag, 2006). In this sense, denser gyro-gyral long-range connections might endow gyri with a plausible role as "hubs" of a structural network, which has been demonstrated in Zhang *et al.* (2020) (Fig. 2D), and will be revealed by functional connectivity/network analyses in the section of 'Gyro-Sulcal Functional Differences from Various Perspectives'.

Support from cross-species comparative studies on brain structure

The complexity of cortical convolution increases generally along the phylogenetic tree and is usually related to species intelligence (Roth and Dicke, 2005). Thus, identifying species-preserved and -specific anatomy and function is a unique and important approach to understanding the development of cortical folding, as well as its relation to structural and functional architectures (Orban *et al.*, 2004; Rilling *et al.*, 2008; de Schotten *et al.*, 2012; Chen *et al.*, 2013; Zhang *et al.*, 2013; Zhang *et al.*, 2014; Li *et al.*, 2017; de Schotten *et al.*, 2019; Eichert *et al.*, 2020).

By limiting our interests to gyro-sulcal patterns, we have found that denser long-range axons between gyri in the section of 'Neuronal processes and gyro-sulcal functional differentiation' are preserved across humans and other primate species such as chimpanzees, macaques, and marmosets (Nie *et al.*, 2012; Chen *et al.*, 2013; Zhang *et al.*, 2014; Li *et al.*, 2020a), as well as in other mammalian species such as ferrets (Xu *et al.*, 2010) and even mice (cerebellum, Zeng *et al.*, 2015). In addition, cross-species comparative studies have revealed that U-shaped short-range fibers coursing along sulcal fundi comprise a larger portion of the human brain relative to that of chimpanzees and macaques (Zhang *et al.*, 2014). In Chen *et al.*(2013) the elaboration and complexity of gyral folding increases from macaque to human and is positively correlated with an increase in the complexity of axons connected to these gyri. These observations have led to a hypothesis that gyral folding and fiber connection patterns "co-evolve" in primate brainsl (Chen *et al.*, 2013). This co-evolution of gyral folding and fiber connection patterns is also related to the evolution of brain function. For example, de Schotten *et al.* (2012) and Rilling *et al.* (2008) found major differences between human and non-human primates in the arcuate fasciculus that may underlie language function. A graph analysis in Zhang *et al.* (2020) has also revealed that, in contrast to sulci, gyri play an increasingly important role in core cortico-cortical networks across non-human and human primates. Taken together, these cross-species studies, although in their infancy, suggest that gyro-sulcal patterns are critical to cortical adaption along the phylogenetic tree and strongly related to the evolution of brain structural/functional organization, cognition, and behavior (Roth and Dicke, 2005; Eichert *et al.*, 2020).

Gyro-Sulcal Functional Differences from Various Perspectives

By adopting the methods of sulci/gyri definition and labeling in individual brains in the section of 'Gyral/Sulcal Definition and Labeling Scheme in Individual Brains' and further co-registering the individual volumetric fMRI to the structural data, the fMRI signals of gyri/sulci in the volume space were mapped and separated (Deng *et al.*, 2014). The fMRI signals of gyri/sulci in the cortical space were also separated via mapping the co-registered fMRI signals onto the cortical surface or directly adopting the HCP grayordinate fMRI data.

Gyro-sulcal functional activity time-frequency differences

The human brain is considered to be a multi-frequency oscillation system (Deco *et al.*, 2017), in which high-frequency activity may reflect local domain cortical processing, and low-frequency activity synchronization across distributed brain regions (von Stein and Sarnthein, 2000; Buzsáki and Draguhn, 2004; Canolty and Knight, 2010; Siegel *et al.*, 2012; Buzsáki *et al.*, 2013). While the conventional temporal resolution of fMRI with a repetition time (TR) of 2 s corresponding to a sampling frequency of 0.5 Hz has warranted the gyro-sulcal functional activity time-frequency analysis without bias (Zhang *et al.*, 2018a; Ge *et al.*, 2019), the development of *in vivo* fMRI techniques has significantly improved fMRI signal temporal resolution and further facilitated the analysis in wider frequency bands of brain activity. For example, the HCP fMRI data (Barch *et al.*, 2013; Smith *et al.*, 2013) has a TR of 0.72 s corresponding to a sampling frequency of 1.39 Hz, which covers multiple frequency

bands of brain activity (0.01–0.027, 0.027–0.073, 0.073–0.198, 0.198–0.5, and 0.5–0.69 Hz) based on previous electrophysiological studies (Penttonen and Buzsáki, 2003; Buzsáki *et al.*, 2013). Investigating the potential time-frequency differences between gyro-sulcal fMRI signals has therefore received increasing interest.

Fast Fourier transformation has commonly been used in previous studies for calculating the power spectrum of gyral/sulcal signals (Zhang *et al.*, 2018a; Ge *et al.*, 2019; Liu *et al.*, 2019; Jiang *et al.*, 2020). The power spectrum distribution characteristics across different frequency bands, as well as other measures (e.g. "1/ƒ" characteristic of the power spectral density plot) have been analyzed and compared between gyro-sulcal signals (Zhang *et al.*, 2018a; Ge *et al.*, 2019; Liu *et al.*, 2019; Jiang *et al.*, 2020). Wavelet entropy (Mallat, 1989; Coifman and Wickerhauser, 1992; Daubechies, 1992; Sang *et al.*, 2011) analysis has also been used (Liu *et al.*, 2019), which quantifies the degree of temporal signal complexity, with higher entropy indicating a more complex signal temporal pattern (Sang *et al.*, 2011).

With the rapid development of deep learning techniques (LeCun *et al.*, 2015) in medical image analysis studies (Litjens *et al.*, 2017; Shen *et al.*, 2017), the convolutional neural network (CNN) has also been adopted for gyral/sulcal fMRI signal analysis given its ability in learning meaningful and discriminative features from raw data as well as class-specific and nonlinearly distributed features of signals in different frequency scales (Golik *et al.*, 2015; Zhou *et al.*, 2016; Huang *et al.*, 2017). Liu *et al.* (2019) performed one of the earliest studies using a CNN-based classifier to reveal differences in gyro-sulcal functional activities based on HCP grayordinate rs-fMRI and t-fMRI BOLD signals. In another study (Zhang *et al.*, 2018a), the CNN-based classification model was modified by adding more convolution layers to improve the classification accuracy of volumetric fMRI data. Macaque rs-fMRI data was also used for cross-species studies (Zhang *et al.*, 2018a). In a recent study (Ge *et al.*, 2019), the CNN-based model was adopted on both healthy people and autism spectrum disorder (ASD) patients. Finally, a more recent study (Jiang *et al.*, 2020) adopted a region-specific one-dimensional CNN model to investigate the characteristics of such gyro-sulcal functional activity differences within each brain region instead of in the whole brain.

The gyral and sulcal t-fMRI/rs-fMRI signals (TR ranges from 0.72 to 2 s) can be effectively differentiated based on the proposed time-frequency-based analysis as well as deep-learning-based approaches (Zhang *et al.*, 2018a; Ge *et al.*, 2019; Liu *et al.*, 2019; Jiang *et al.*, 2020). Moreover, as shown in Fig. 3A, the sulcal t-fMRI/rs-fMRI signals have been found to have more diverse temporal patterns as well as higher frequency than gyral signals at the whole-brain level (Zhang *et al.*, 2018a; Ge *et al.*, 2019; Liu *et al.*, 2019), which has been validated by an independent wavelet entropy analysis (Liu *et al.*, 2019). A recent study (Jiang *et al.*, 2020) further found that gyral/sulcal signals could be differentiated within each brain region, and that

gyral/sulcal temporal patterns have different frequency scale characteristics across different brain regions.

Gyro-sulcal functional connectivity/interaction differences

Functional connectivity (FC) is used to characterize functional integration and is defined as statistical dependencies among remote brain regions (Friston, 2011). One of the most commonly used measures of FC is the Pearson correlation coefficient (PCC), which calculates the temporal correlation of fMRI BOLD signals between voxels or brain regions (Fox and Raichle, 2007). A larger coefficient value represents stronger FC, and vice versa.

Deng *et al.* (2014) performed one of the earliest FC studies to investigate gyro-sulcal FC differences. They first focused on the primary motor and somatosensory systems as a test bed example, since these systems are proven to be structurally and functionally connected (Kandel *et al.*, 2000). It has been found that within the primary motor and somatosensory systems, including four gyral regions (bilateral precentral gyrus and postcentral gyrus) and four sulcal regions (bilateral central sulcus and postcentral sulcus), the rs-FC strength is strong between gyro-gyral regions, moderate between gyro-sulcal regions, and weak between sulco-sulcal regions (Fig. 3B). Deng *et al.* (2014) further performed whole-brain analysis based on the A-DICCCOL (anatomy-guided dense individualized and common connectivity-based cortical landmarks) system (Jiang *et al.*, 2015b), which defined 555 cortical landmarks on 68 major gyral/sulcal regions in the whole cerebral cortex, and obtained a similar gyro-sulcal rs-FC difference. In another study (Liu *et al.*, 2017), the task-based FC was calculated using the PCC of t-fMRI temporal patterns between any pair of gyral/sulcal components, and found to be stronger in gyro-gyral than in sulco-sulcal regions in the whole brain across the seven different tasks of the HCP. In addition to investigating static FC by averaging scan-length rs-fMRI/t-fMRI time series (Deng *et al.*, 2014; Liu *et al.*, 2017), the temporal-varying dynamic FC differences between gyri and sulci have also been explored (Yang *et al.*, 2019). The FC dynamic temporal variability within or between brain regions has been extensively demonstrated (Gilbert and Sigman, 2007; Chang and Glover, 2010; Smith *et al.*, 2011; Calhoun *et al.*, 2014; Li *et al.*, 2014; Ou *et al.*, 2014; Yuan *et al.*, 2018). In Yang *et al.*, 2019, the rs-fMRI BOLD signals were divided into non-overlapping time windows, and the temporal-varying FC dynamics of each gyral/sulcal region assessed by means of calculating the variance of the PCC of BOLD signals between any pair of time windows, to allow differences between gyri and sulci to be examined. It has been found that the dynamic temporal variance of the rs-fMRI signal was larger in gyral than in sulcal regions in the whole brain (Yang *et al.*, 2019). Instead of assessing the FC between gyro-sulcal regions directly (Deng *et al.*, 2014; Liu *et al.*, 2017; Yang *et al.*, 2019), another study explored
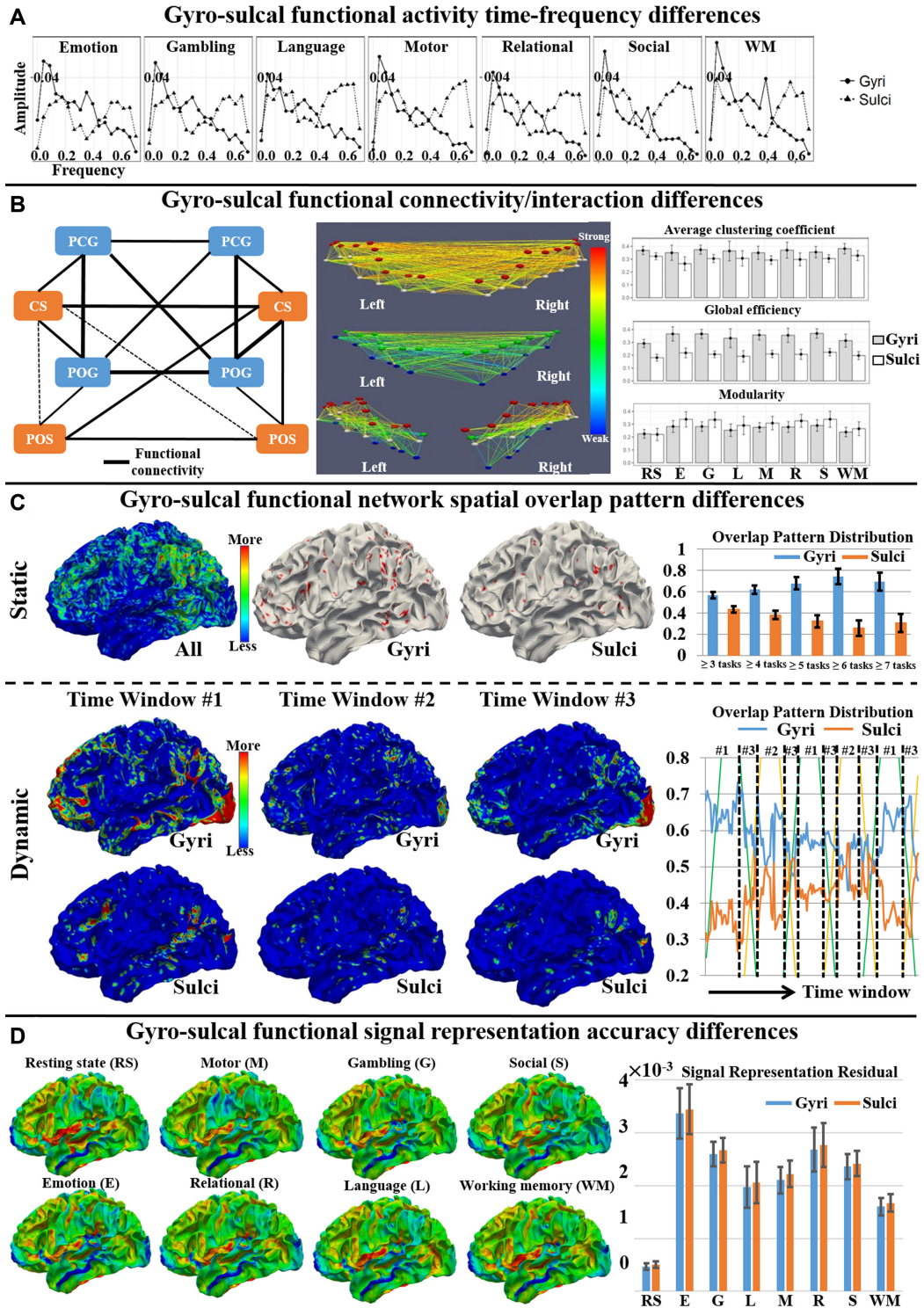
Figure 3: Summary of gyro-sulcal functional differences. (**A**) Gyro-sulcal functional activity time-frequency difference. The average power spectrum of gyral and sulcal temporal patterns is shown in the seven t-fMRI data sets from the HCP, which is adapted from Liu *et al.* (2019). (**B**) Gyrosulcal functional connectivity/interaction difference. The left sub-figure shows the gyro-sulcal functional connectivity (black edges) within the primary motor and somatosensory system. Thicker edges represent stronger connections. The middle sub-figure shows the gyro-sulcal functional connectivity patterns of one example participant. The red, white, green, and blue bubbles represent the ROI on PCG, POG, CS, and POS, respectively. The edges are colored based on the functional connectivity strength. The left and middle sub-figures are adapted from Deng *et al.* (2014). The right sub-figure shows the graph-theory-based property difference of gyro-sulcal functional connectivity, which is adapted from Liu *et al.* (2017). (**C**) Gyro-sulcal functional network spatial overlap pattern difference. The static gyro-sulcal overlap pattern difference across multiple tasks is adapted from Jiang *et al.* (2015a). The temporal dynamics of gyro-sulcal overlap pattern difference in Emotion task from the HCP is adapted from Jiang *et al.* (2018a). (**D**) Gyro-sulcal functional signal representation accuracy difference. The gyro-sulcal signal representation residual is shown across the eight fMRI from the HCP, which is adapted from Zhao *et al.* (2020).

the differential FC of gyri/sulci with other brain regions (Uddin *et al.*, 2010). It has been found that the angular gyrus and the intraparietal sulcus, which are a part of the inferior parietal lobule, have differential rs-FCs with other brain regions (Uddin *et al.*, 2010). Other measures have also been used to characterize functional interaction by quantifying the temporal correlation of fMRI signals. (Li *et al.*, 2013) adopted a cross wavelet transform to measure the functional interaction between two regions. The functional interaction strength was defined as the locations where both signals shared high co-power in the time-frequency domain, and the gyro-sulcal difference was then obtained (Li *et al.*, 2013).

Based on the FC/functional interaction network among gyral/sulcal regions, some studies have further adopted graph theory-based properties (Bullmore and Sporns, 2009; Rubinov and Sporns, 2010) to investigate the functional integration/segregation of such FC/functional interaction networks as well as their differences between gyri and sulci (Li *et al.*, 2013; Deng *et al.*, 2014; Liu *et al.*, 2017). First, the FC/functional interaction networks were constructed within gyral/sulcal/mixed (both gyral and sulcal) brain regions, respectively. Second, certain graph theory-based properties such as edge degree, global efficiency, modularity, small-worldness, etc. were measured and compared among those networks. It has been found that the resting state functional interaction network composed of gyral regions has higher global and local economical properties, and stronger small-worldness and functional interaction strength than the sulcal network (Li *et al.*, 2013). Within the rs-FC network, the graph edge degree of the gyral regions is significantly higher than that of the sulcal regions (Deng *et al.*, 2014). Liu *et al.* (2017) have found that the FC network composed of gyral regions has higher average cluster coefficients and global efficiency than those of sulcal regions in both rs-fMRI and the seven t-fMRI data (Fig. 3B). In terms of modularity property, the sulcal network is significantly higher than the gyral one in t-fMRI but not rs-fMRI data (Liu *et al.*, 2017).

Gyro-sulcal functional network spatial overlap pattern differences

The functional network spatial overlap pattern is defined as the set of brain regions that are spatially overlapped and involved in multiple brain networks. Previous studies have demonstrated extensively that there are multiple spatially overlapped brain functional networks that are interacting with each other (Bullmore and Sporns, 2009; Lv *et al.*, 2014, 2015). The functional network spatial overlap pattern thus represents the higher-order brain regions that are involved in multiple cognitive tasks.

Sparse coding has been widely used for rs-fMRI and t-fMRI analysis to infer brain functional characteristics including the functional network spatial overlap pattern

(Abolghasemi *et al.*, 2015; Lv *et al.*, 2014, 2015). The whole-brain fMRI BOLD signals are denoted as a matrix $\mathbf{X} = [\mathbf{x}_1, \mathbf{x}_2, \ldots, \mathbf{x}_n] \in \mathbb{R}^{t \times n}$, in which $\mathbf{x}_n$ is the fMRI BOLD signal of voxel n normalized to zero mean and standard deviation of 1 (Mairal *et al.*, 2010), t is the length of the fMRI signal. By applying the online dictionary learning/sparse coding approach (Mairal *et al.*, 2010), $\mathbf{X}$ is represented as

$$\mathbf{X} = \mathbf{D} \times \alpha + \varepsilon \qquad (1)$$

where $\mathbf{D} = [\mathbf{d}_1, \mathbf{d}_2, \ldots, \mathbf{d}_m] \in \mathbb{R}^{t \times m}$ (m denotes dictionary size, $m > t$ and $m << n$) is an over-complete dictionary matrix, $\boldsymbol{\alpha} = [\boldsymbol{\alpha}_1, \boldsymbol{\alpha}_2, \ldots, \boldsymbol{\alpha}_n] \in \mathbb{R}^{m \times n}$ is a sparse coefficient matrix, and ε is error term. Each fMRI signal $\mathbf{x}_i$ is represented as $\overline{\mathbf{x}_i} = \mathbf{D} \times \boldsymbol{\alpha}_i + \boldsymbol{\varepsilon}$. Note that each column of $\mathbf{D}$ ($\mathbf{d}_m$) is a basis functional temporal pattern which is representative of whole-brain fMRI BOLD signals, and each row of $\boldsymbol{\alpha}$ represents the spatial pattern of the functional network that corresponds to the basis temporal pattern. The meaningful functional network spatial overlap patterns can then be effectively identified (Zhang W. *et al.*, 2019).

Using sparse coding approaches, Jiang *et al.* (2015a) characterized task-based heterogeneous functional regions (THFRs), which represented those higher-order brain regions involved in multiple cognitive tasks, based on all identified task-evoked and intrinsic functional network patterns. It has been found that both task-evoked and intrinsic connectivity functional networks can be effectively and robustly identified across the seven different t-fMRI of HCP grayordinate data (Jiang *et al.*, 2015a). Moreover, the THFRs are located more on gyral than on sulcal regions within the bilateral parietal lobe, frontal lobe, and visual association cortices across different t-fMRI data (Fig. 3C). To further investigate the temporal dynamics of THFRs [i.e. spatial overlap patterns of functional networks (SOPFNs)] on gyri/sulci, SOPFNs and their spatial distribution proportion on gyri/sulci were identifed based on t-fMRI data within each sliding time window (Jiang *et al.*, 2018a). It has been shown that the SOPFNs are also located more on gyral than on sulcal regions within bilateral parietal lobe, frontal lobe, and visual association cortices within each time window, and it is of interest that there is variability in the SOPFNs distribution percentage between gyri and sulci across different time windows (Fig. 3C). Specifically, the SOPFNs distribution percentage value of gyral regions was increased and achieved a peak value during the task blocks of block design t-fMRI, while that of sulcal regions was decreased and reached a trough value during the task blocks. When the task paradigm was changed from a task block to a resting state block, the SOPFNs distribution percentage was decreased from the peak for gyral regions and increased from the trough for sulcal regions, and achieved relatively the same percentage before starting the next task block (Jiang *et al.*, 2018a). These findings were also consistent across the
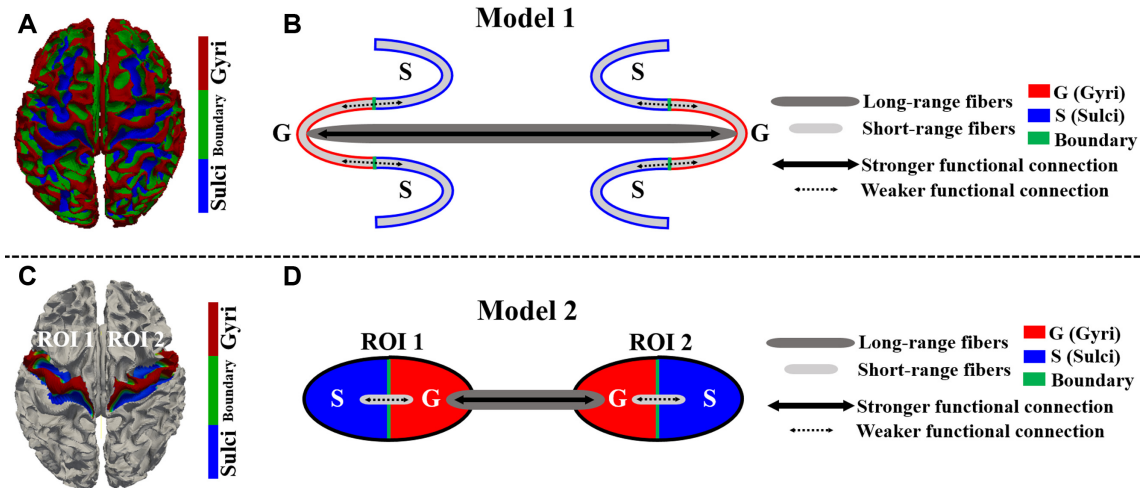
Figure 4: Proposed functional models of gyri and sulci in previous studies. (**A**) The gyri/sulci defined in the whole-brain; (**B**) the proposed functional model of gyri and sulci at the whole-brain scale; and (**C**) an example of a motor functional network with two ROI. Each ROI consists of gyri and sulci. (**D**) The proposed functional model of gyri and sulci within functional networks.

seven different block design t-fMRI of HCP grayordinate data (Jiang *et al.*, 2018a).

Gyro-sulcal functional signal representation accuracy differences

The fMRI signal representation accuracy is defined as the PCC between the original signal x_i and the represented signal $\overline{x_i}$ based on Equation (1) (Jiang *et al.*, 2018b). Since sparse coding approaches can compactly represent the original fMRI BOLD signals using the identified small number of basis functional temporal patterns and corresponding functional network patterns, a larger PCC value indicates better representation of x_i as well as better participation of x_i in the neural function during a specific task.

Using nine intrinsic functional networks including default mode, visual, motor, auditory, executive control, and bilateral frontal/parietal networks (Smith *et al.*, 2009), Jiang *et al.* (2018b) assessed and compared the signal representation of emotion processing t-fMRI data between gyral and sulcal regions within each of the nine networks. It has been found that during the emotion processing, gyral regions have better signal representation accuracy than sulcal regions within the nine intrinsic functional networks. In another recent study (Zhao *et al.*, 2020), the signal representation accuracy was defined as the residual between the original signal x_i and the represented signal $\overline{x_i}$. Inversely, a smaller value of the residual indicates better representation of x_i. The signal representation accuracy was further assessed and compared between gyral and sulcal regions within the nine intrinsic functional networks under both the resting state and seven different assessment tasks including assessment of emotions, gambling, language, motor skills, relational skills, social skills, and working memory from the HCP. The variability magnitude of such

gyro-sulcal differences was also assessed across different tasks/resting state and in intrinsic functional networks (Fig. 3D). It has been found that gyral regions consistently have better signal representation accuracy than sulcal regions within all nine intrinsic functional networks across all seven different t-fMRI of HCP grayordinate data. Moreover, the magnitudes of such gyro-sulcal differences vary across resting state/tasks and intrinsic functional networks. Specifically, in the resting state and "low-demand" tasks such as motor tasks, the gyro-sulcal signal representation accuracy contrast values are lowest and more consistent within the nine intrinsic networks as well as the whole-brain level across different participants. On the contrary, the gyro-sulcal contrast is higher in "high-demand" tasks, such as language and social and working memory, and less consistent across different participants. Moreover, the gyro-sulcal signal representation accuracy contrast is more pronounced within the default mode and executive control networks compared to the other intrinsic functional networks in all seven tasks, while it is the lowest within the sensorimotor network across all tasks (Zhao *et al.*, 2020).

A Dynamic Functional Model of Gyri and Sulci

We have previously proposed a functional model of gyri and sulci at the whole-brain level (Deng *et al.*, 2014) (Fig. 4B) and within functional networks (Jiang *et al.*, 2018b) (Fig. 4D): individual gyri exchange information with other distant gyri through long-range fibers and with neighboring sulci through short-range fibers, while individual sulci exchange information directly with neighboring gyri through short-range fibers and indirectly with other regions through the neighboring gyri.

However, this model does not explicitly explain how the interplay between gyri and sulci or their resulting dynamic interactions occurs. In this review, we would therefore like to propose a dynamic functional model of gyri and sulci as illustrated in Fig. 5, in which the involvement of gyri and sulci in global functional networks is dynamically balanced analogous to an activator–inhibitor system (Turing, 1952; Meinhardt and Gierer, 1974; Nakamasu *et al.*, 2009; Yagi, 2009). The gyro-sulcal functional differences summarized in the section of 'Gyro-Sulcal Functional Differences from Various Perspectives' and Figs 3 and 4 from various perspectives are the foundation of this dynamic model. Compared with sulci, gyri have less diverse temporal patterns as well as lower frequency of fMRI signals, higher static or dynamic resting state/task-based FC, different graph-theory-based properties (higher global/local economical properties, graph edge degree, average cluster coefficient, and global efficiency; stronger small-worldness, and functional interaction), a greater distribution of THFRs and SOPFNs, and a higher signal representation accuracy. In the dynamic model in Fig. 5, when the task in a block design t-fMRI is loaded onto brain networks the gyri are activated. The SOPFNs distribution percentage of gyri begins to increase and achieves a peak value analogous to an activator since gyri are hypothesized to be the global functional center, while that of sulci begins to be inhibited to decrease and reach a trough value (Fig. 5B). When the task load is removed and the next resting state block starts, the excitatory and inhibitory effects vanish. The SOPFNs distribution percentage of gyri begins to drop from the peak point, while that of sulci begins to increase from the trough, until achieving relatively the same SOPFNs distribution percentage by the end of the resting state block (Fig. 5A). Such a gyro-sulcal dynamic balancing procedure then repeats when the next task block starts (Jiang *et al.*, 2018a). The excitatory and inhibitory effects can be regulated by strong gyro-gyral functional connections and weak gyro-sulcal ones, analogous to an activator-inhibitor regulation system (Turing, 1952; Meinhardt and Gierer, 1974; Nakamasu *et al.*, 2009; Yagi, 2009), underpinned by long-range and short-range axons, respectively, as illustrated in the model in Fig. 4.

As a substrate for the dynamic model, long-range connections and short-range connections are needed to coincide in the axonal system. We have discussed the presence of long-range association projections in the section of 'Neuronal processes and gyro-sulcal functional differentiation', which are usually radial to the cortical surface of two remote gyri. The presence of a short-range axonal system, the connections of which are between two neighboring gyri and superficial to and parallel with the cortical surface, has also been demonstrated (Bullmore and Sporns, 2009; Sepulcre *et al.*, 2010; Reveley, *et al.*, 2015; Yoshino *et al.*, 2020). Although the regulation mechanisms of long- and short-range axons in the dynamic model are still far from being clear, some studies have shown some progress toward achieving this goal. The functional network segregation is suggested to be driven by the abundance of short-range axons (Cao *et al.*, 2017) while the long-range ones are involved in global information integration (Gao *et al.*, 2009). A precise balance between the decreased short-range axon numbers and increased long-range axon numbers from 2 to 7 years in humans (Ouyang *et al.*, 2017) has been shown to be positively associated with the reconfiguration of a developmental functional connectome from segregation to integration (Fair *et al.*, 2009). A disturbance of this balance could result in brain disorders, such as hyperconnectivity for ASD and hypoconnectivity for schizophrenia (SZ) (Ouyang *et al.*, 2017).

It is noteworthy that the excitatory and inhibitory effects might be implemented by the diffusion of functional gradients, as suggested in activator-inhibitor models (Turing, 1952; Meinhardt and Gierer, 1974; Nakamasu *et al.*, 2009; Yagi, 2009). In fact, a global gradient has been observed in the cortex from a variety of perspectives ranging from genes to behavior (Huntenburg *et al.*, 2018). Similarly, a gyro-sulcal gradient could also exist, although it might be overwhelmed by the global one. Indeed, a gradient between gyro-sulcal functional differences has been evidenced. During the dynamic balancing procedure of gyro-sulcal functions, the SOPFNs distribution percentage of gyri/sulci is increased or decreased in a gradient manner along with the task/resting state blocks instead of an abrupt change (Jiang *et al.*, 2018a). Moreover, the gyro-sulcal pattern is associated with the functional localization gradient (Li *et al.*, 2015; Troiani *et al.*, 2020). For instance, it was found that the theoretically proposed rostral-caudal gradient of secondary-primary rewards is consistent with the spatial location of different rewards along a rostral-caudal gradient in the medial orbital sulcus (Li *et al.*, 2015).

The gyro-sulcal gradient could be deeply rooted by a genetic protomap. In fact, a global scale predominant direction of gene expression gradients in the cortex has been widely reported (Miller *et al.*, 2014; Burt *et al.*, 2018; Huntenburg *et al.*, 2018; Fulcher *et al.*, 2019; Li *et al.*, 2020b). In particular, distant cortical regions could also show similar gene expression if they have long-range connections (Richiardi *et al.*, 2015; Krienen *et al.*, 2016). In this sense, it could be inferred that cortical areas sharing a similar structural property could show similar gene expression, which would result in a gene expression gradient along the given structural property. Provided that gyri and sulci are two basic anatomical units of cortical morphology, the existence of a gyro-sulcal gradient is predicted, although overwhelmed by the global diffusion. This inference has gained partial support from several studies where differential expression of a great number of genes between gyri and sulci have been observed (de Juan Romero and Borrell, 2015; Zeng *et al.*, 2015; Li *et al.*, 2020). Some of gene differences already exist in the germinal layers, providing a protomap with abrupt gradients to locations of gyri and sulci that develop later (de Juan Romero and Borrell, 2015).
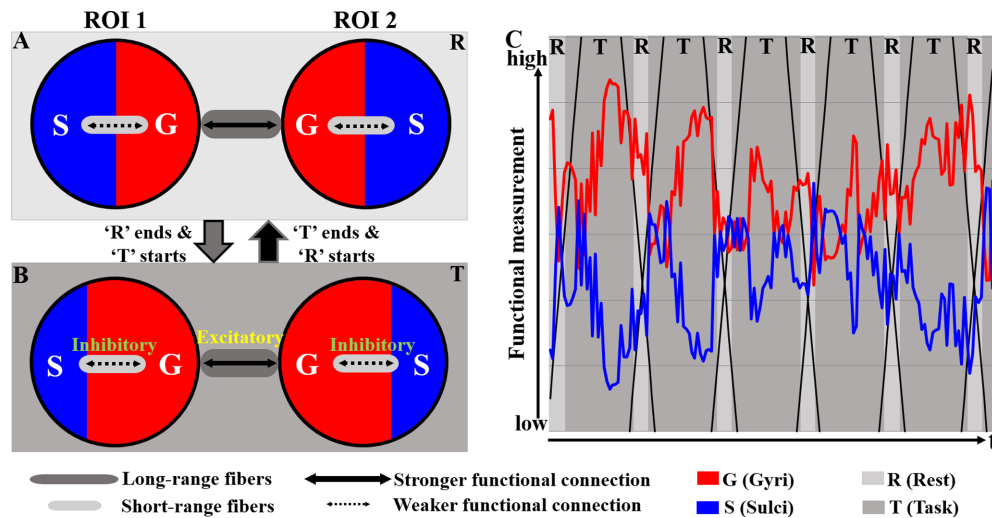
Figure 5: (**A**) and (**B**) An illustration of the dynamic functional model of gyri and sulci, at resting state (A) and during task performance (B). Two ROI as well as their connections are used to represent the whole-brain network. Areas of the gyri and sulci within each ROI illustrate the degree of involvement in global networks. The thickness of the double-head arrows illustrate the excitatory (thick) and inhibitory (thin) effects, putatively regulated by functional connections. (**C**) The degrees of involvement in global networks of gyri (red) and sulci (blue) during a task performance (Jiang *et al.*, 2018a).

Future Research Directions

Definitions of gyri and sulci

As demonstrated in the section of 'Definition of gyri and sulci', gyri and sulci are usually treated as morphological and anatomical nomenclature. However, it is not clear how to define their morphological boundary. For example, if the zero level of convexity in FreeSurfer is used as a strict gyro-sulcal boundary, gyri below it would be defined as sulci. In this respect, it is difficult to define a clear boundary, if any, between gyri and sulci. Also, a group of gyri, termed *pli de paset a* (Gratiolet, 1854; Parent, 2014), were found to be buried in the depth of sulci and interrupting the continuity of the sulci, challenging the conventional definition of gyri, as being in continuity with each other across the entire cortex. Because of their specialty, pli de passage are suggested as benchmarks for cortical folding development modeling (Regis *et al.*, 2005; Mangin *et al.*, 2019) and a linkage between gyral and sulcal systems.

In this review, we have discussed the possibility of a mapping between gyro-sulcal patterns and functions and suggest that these two anatomical patterns could serve as basic blocks for a complex building of brain functions. Although conventional definitions of gyri and sulci are used in these studies, it is thought provoking that definitions could be revised by integrating axonal wiring and function information (Zhu *et al.*, 2013; Jiang *et al.*, 2015b; Lv *et al.*, 2014, 2015; Zhang *et al.*, 2018b, 2019a, b). For example, Jiang *et al.* (2015b) proposed 555 cortical landmarks on major cortical regions with gyro-sulcal anatomical and fiber connection correspondences across different participants. Zhang *et al.* (2018b, 2019a, b) further combined functional, structural, and anatomical

information to identify cortical landmarks across participants. More effort needs to be devoted in the future to systematically investigate the gyro-sulcal definitions as well as their influences on functional models of gyri and sulci.

Gyro-sulcal framework is far from being sufficient

Another important question that needs to be asked is, are gyri and sulci the ultimate basic units for deciphering cortical morphology and anatomo-function relation, or can they be sub-divided? In fact, a group of studies (Lohmann *et al.*, 2008; Im *et al.*, 2010, 2011; Meng *et al.*, 2014) have particularly focused on the deepest local regions of sulci, termed sulcal pits, the spatial placements of which remain invariant during brain growth. This invariance is closely related to intellectual ability (Im *et al.*, 2011) and a protomap of functional areas (Lohmann *et al.*, 2008; Im *et al.*, 2010). In our studies, we have defined a novel gyral folding pattern (Li K. *et al.*, 2010), termed the gyral hinge, which is the conjunction of multiple gyri from different directions. Gyral hinges are distinguished from other gyral regions because they have the thickest cortices, the strongest long-range axonal connections, the most aggregative functional profiles (Li K. *et al.*, 2010; Yu *et al.*, 2013; Chen *et al.*, 2014; Jiang *et al.*, 2015a, 2018a; Li *et al.*, 2017; Ge *et al.*, 2018), and comprise a majority portion of the cortico-cortical network's "core" (Zhang *et al.*, 2020). Taken together, these studies indicate that classic gyro-sulcal patterns could be further sub-divided to meaningful units, such as ordinary sulci, ordinary gyri, sulcal pits, and gyral hinges.

Importance and necessity of considering gyro-sulcal functional differences in brain disorder studies

Size, morphology, and spatial patterns of cortical folding have been related to various brain functions (Barkovich et al., 2012; Fernández et al., 2016). Abnormalities and changes in cortical folding have been reported to lead to severe brain malfunctions and problems in intellectual and cognitive functioning (Barkovich et al., 2012; Fernández et al., 2016). Some congenital cortical abnormalities, such as lissencephaly, microcephaly, and polymicrogyria, provide extreme examples of associations with severe anatomical pathology and mental deficits (Richman et al., 1974; Richman et al., 1975; Stutterd and Leventer, 2014; Di Donato et al., 2017: for a full review of these findings, see Fernández et al., 2016). Moreover, mild folding abnormalities, in developmental psychiatric disorders such as ASD and SZ, are also associated with cognition and behavioral impairments (White et al., 2003; Nordahl et al., 2007; Csernansky et al., 2008; Blanken et al., 2015; Dierker et al., 2015; Ecker et al., 2015). In ASD, these include deficits in social communication, social reciprocity, and repetitive and stereotyped behaviors and interests (Wing, 1997), and in attention, memory, social withdrawal and executive functions in SZ (Gur et al., 2000; Goldberg, 2003). Patients with ASD have also been reported to exhibit polymicrogyria, schizencephaly, and microgyria in the cortex (Piven et al., 1990). In particular, some sulci, such as the Sylvian fissure, are elongated (Levitt et al., 2003) and the gyrification of the frontal lobe is increased (Hardan et al, 2004). Similarly, in SZ patients, widespread abnormalities in cortical folding patterns have also been reported (Narr et al., 2004; Arnold et al., 2005) including in the temporal lobes (Kikinis et al., 1994) and frontal, occipital, and parietal cortices (Shenton et al., 2001; Narr et al., 2004).

A number of studies have focused on gyro-sulcal patterns with the aim of providing a more precise anatomo-functional mapping of potential contributions to mental disorders (reviewed by Nakamura et al., 2020). These studies have developed an approach for extracting gyro-sulcal patterns according to their spatial topology. In these studies, a set of H-shaped sulci in the orbito-frontal cortex (OFC) was of major interest because of its linkage with cognitive and social deficits in a variety of brain disorders (Ongur and Price, 2000). The OFC gyro-sulcal pattern has been classified into three types (Chiavaras and Petrides, 2000—type I, type II, and type III in order of frequency). In general, in type I the lateral orbital sulci (LOS) are continuous while the medial orbital sulci (MOS) are interrupted; in type II, both LOS and MOS are continuous; and in type III, both LOS and MOS are interrupted. It was found that the most common type I expression in healthy controls was decreased while the least common type III expression in healthy controls was increased in SZ (Nakamura et al., 2007). Similar atypical distributions of the gyro-sulcal patterns have been reported in ASD (Watanabe et al., 2014), attention deficit/hyperactivity disorder (ADHD), and bipolar disorder (BD) (Patti and Troiani, 2018).

However, most of those studies only focus on general morphological measures such as the gyrification index, cortical area, etc., while gyro-sulcal functional difference characteristics have received far less attention in existing human behavior and brain disorder studies. Conventional cognitive, psychological, and psychiatric studies usually select a large brain region of interest (ROI) (e.g. prefrontal cortex) based on an available brain atlas that neglects gyro-sulcal functional differences within it. As a consequence, subsequent ROI-based analyses (e.g. activation detection, FC analysis) are therefore inaccurate and may lose useful findings or generate false positive ones, especially when performing between-group comparisons. Since a number of mental disorder studies have demonstrated the possibility that gyro-sulcal topological patterns could be used as a proxy for brain functions and cognition (Nakamura et al., 2020; Troiani et al., 2020), it may be more important to use gyro-sulcal functional patterns as neurodevelopmental markers for future brain disorder diagnosis, cognitive, psychological, and psychiatric studies to obtain more accurate and reliable findings.

Author contributions

Conflict of interests

Acknowledgements

References

Abolghasemi V, Ferdowsi S, Sanei S (2015) Fast and incoherent dictionary learning algorithms with application to fMRI. *SIViP* **9**:147–58.

Amiez C, Kostopoulos P, Champod AS, *et al.* (2006) Local morphology predicts functional organization of the dorsal premotor region in the human brain. *J Neurosci* **26**:2724–31.

Amiez C, Neveu R, Warrot D, *et al.* (2013) The location of feedback-related activity in the midcingulate cortex is predicted by local morphology. *J Neurosci* **33**:2217–28.

Amiez C, Petrides M (2014) Neuroimaging evidence of the anatomo-functional organization of the human cingulate motor areas. *Cereb Cortex* **24**:563–78.

Amiez C, Petrides M (2018) Functional rostro-caudal gradient in the human posterior lateral frontal cortex. *Brain Struct Funct* **223**:1487–99.

Arnold SE, Talbot K, Hahn CG (2005) Neurodevelopment, neuroplasticity, and new genes for schizophrenia. *Prog Brain Res* **147**:319–45.

Barch DM, Burgess GC, Harms MP, *et al.* (2013) Function in the human connectome: task-fMRI and individual differences in behavior. *Neuroimage* **80**:169–89.

Barkovich AJ, Guerrini R, Kuzniecky RI, *et al.* (2012) A developmental and genetic classification for malformations of cortical development: update 2012. *Brain* **135**:1348–69.

Bayly P, Okamoto R, Xu G, *et al.* (2013) A cortical folding model incorporating stress-dependent growth explains gyral wavelengths and stress patterns in the developing brain. *Phys Biol* **10**:016005.

Behnke KJ, Rettmann ME, Pham DL, *et al.* (2003) Automatic classification of sulcal regions of the human brain cortex using pattern recognition. *Proceedings of SPIE* **5032**:1499–510.

Benson NC, Butt OH, Datta R, *et al.* (2012) The retinotopic organization of striate cortex is well predicted by surface topology. *Curr Biol* **22**:2081–5.

Betizeau M, Cortay V, Patti D, *et al.* (2013) Precursor diversity and complexity of lineage relationships in the outer subventricular zone of the primate. *Neuron* **80**:442–57.

Biswal B, Yetkin FZ, Haughton VM, *et al.* (1995) Functional connectivity in the motor cortex of resting human brain using echo-planar MRI. *Magn Reson Med* **34**:537–41.

Blanken LM, Mous SE, Ghassabian A, *et al.* (2015) Cortical morphology in 6-to 10-year old children with autistic traits: a population-based neuroimaging study. *AJP* **172**:479–86.

Borrell V, Götz M (2014) Role of radial glial cells in cerebral cortex folding. *Curr Opin Neurobiol* **27**:39–46.

Brodmann K (1909) *Vergleichende Lokalisationslehre der Grosshirnrinde in ihren Prinzipien dargestellt auf Grund des Zellenbaues.* *Leipzig*: Barth.

Budde MD, Annese J (2013) Quantification of anisotropy and fiber orientation in human brain histological sections. *Front. Integr. Neurosci.* **7**:3.

Bullmore E, Sporns O (2009) Complex brain networks: graph theoretical analysis of structural and functional systems. *Nat Rev Neurosci* **10**:186–98.

Bullmore E, Sporns O (2012) The economy of brain network organization. *Nat Rev Neurosci* **13**:336–49.

Burt JB, Demirtaş M, Eckner WJ, *et al.* (2018) Hierarchy of transcriptomic specialization across human cortex captured by structural neuroimaging topography. *Nat Neurosci* **21**:1251–9.

Buzsáki G, Draguhn A (2004) Neuronal oscillations in cortical networks. *Science* **304**:1926–9.

Buzsáki G, Logothetis N, Singer W (2013) Scaling brain size, keeping timing: evolutionary preservation of brain rhythms. *Neuron* **80**:751–64.

Cachia A, Mangin JF, Rivière D, *et al.* (2003a) A primal sketch of the cortex mean curvature: a morphogenesis based approach to study the variability of the folding patterns. *IEEE Trans Med Imaging* **22**:754–65.

Cachia A, Mangin JF, Rivière D, *et al.* (2003b) A generic framework for the parcellation of the cortical surface into gyri using geodesic Voronoï diagrams. *Med Image Anal* **7**:403–16.

Cachia A, Roell M, Mangin J-F, *et al.* (2018) How interindividual differences in brain anatomy shape reading accuracy. *Brain Struct Funct* **223**:701–12.

Calhoun VD, Miller R, Pearlson G, *et al.* (2014) The chronnectome: time-varying connectivity networks as the next frontier in fMRI data discovery. *Neuron* **84**:262–74.

Canolty RT, Knight RT (2010) The functional role of cross-frequency coupling. *Trends Cogn Sci* **14**:506–15.

Cao M, He Y, Dai Z, *et al.* (2017) Early development of functional network segregation revealed by connectomic analysis of the preterm human brain. *Cereb Cortex* **27**:1949–63.

Chang C, Glover GH (2010) Time–frequency dynamics of resting-state brain connectivity measured with fMRI. *Neuroimage* **50**:81–98.

Chen H, Zhang T, Guo L, *et al.* (2013) Coevolution of gyral folding and structural connection patterns in primate brains. *Cereb Cortex* **23**:1208–17.

Chen H, Yu X, Jiang X, *et al.* (2014) Evolutionarily-preserved consistent gyral folding patterns across primate brains. *IEEE 11th International Symposium on Biomedical Imaging (ISBI)* 1218–21.

Chi JG, Dooling EC, Gilles FH (1977) Gyral development of the human brain. *Ann Neurol* **1**:86–93.

Chiavaras MM, Petrides M (2000) Orbitofrontal sulci of the human and macaque monkey brain. *J Comp Neurol* **422**:35–54.

Chklovskii DB, Schikorski T, Stevens CF (2002) Wiring optimization in cortical circuits. *Neuron* **34**:341–7.

Coifman RR, Wickerhauser MV (1992) Entropy-based algorithms for best basis selection. *IEEE Trans Inform Theory* **38**:713–8.

Collins DL, Goualher GL, Evans AC (1998) Non-linear cerebral registration with sulcal constraints. *Int Conf Med Image Comput Comput Assist Interv* 974–84.

Csernansky JG, Gillespie SK, Dierker DL, *et al.* (2008) Symmetric abnormalities in sulcal patterning in schizophrenia. *Neuroimage* **43**:440–6.

Daubechies I (1992) *Ten Lectures on Wavelets: SIAM.*

Davatzikos C (1997) Spatial transformation and registration of brain images using elastically deformable models. *Comput Vision Image Understanding* **66**:207–22.

de Juan Romero C, Borrell V (2015) Coevolution of radial glial cells and the cerebral cortex. *Glia* **63**:1303–19.

Desai R, Liebenthal E, Possing ET, *et al.* (2005) Volumetric vs. surface-based alignment for localization of auditory cortex activation. *Neuroimage* **26**:1019–29.

de Schotten MT, Dell'Acqua F, Valabregue R, *et al.* (2012) Monkey to human comparative anatomy of the frontal lobe association tracts. *Cortex* **48**:82–96.

de Schotten MT, Croxson PL, Mars RB (2019) Large-scale comparative neuroimaging: where are we and what do we need? *Cortex* **118**:188–202.

Deco G, Cabral J, Woolrich MW, *et al.* (2017) Single or multiple frequency generators in on-going brain activity: a mechanistic whole-brain model of empirical MEG data. *Neuroimage* **152**:538–50.

Deng F, Jiang X, Zhu D, *et al.* (2014) A functional model of cortical gyri and sulci. *Brain Struct Funct* **219**:1473–91.

Desikan RS, Se´gonne F, Fischl B, *et al.* (2006) An automated labeling system for subdividing the human cerebral cortex on MRI scans into gyral based regions of interest. *Neuroimage* **31**:968–80.

Di Donato N, Chiari S, Mirzaa GM, *et al.* (2017) Lissencephaly: expanded imaging and clinical classification. *Am J Med Genet* **173**:1473–88.

Dierker DL, Feczko E, Pruett, JR, Jr, *et al.* (2015) Analysis of cortical shape in children with simplex autism. *Cereb Cortex* **25**:1042–51.

Dubois J, Benders M, Borradori-Tolsa C, *et al.* (2008) Primary cortical folding in the human newborn: an early marker of later functional development. *Brain* **131**:2028–41.

Dubois J, Dehaene-Lambertz G, Kulikova S, *et al.* (2014) The early development of brain white matter: a review of imaging studies in fetuses, newborns and infants. *Neuroscience* **276**: 48–71.

Ecker C, Bookheimer SY, Murphy DG (2015) Neuroimaging in autism spectrum disorder: brain structure and function across the lifespan. *The Lancet Neurology* **14**:1121–34.

Eichert N, Robinson EC, Bryant KL, *et al.* (2020) Cross-species cortical alignment identifies different types of anatomical reorganization in the primate temporal lobe. *eLife* **9**:e53232.

Englund C, Fink A, Lau C, *et al.* (2005) Pax6, Tbr2, and Tbr1 are expressed sequentially by radial glia, intermediate progenitor cells, and postmitotic neurons in developing neocortex. *J Neurosci* **25**:247–51.

Fair DA, Cohen AL, Power JD, *et al.* (2009) Functional brain networks develop from a "local to distributed" organization. *PLoS Comput Biol* **5**:e1000381.

Fernández V, Llinares-Benadero C, Borrell V (2016) Cerebral cortex expansion and folding: what have we learned? *EMBO J* **35**:1021–44.

Fietz SA, Kelava I, Vogt J, *et al.* (2010) OSVZ progenitors of human and ferret neocortex are epithelial-like and expand by integrin signaling. *Nat Neurosci* **13**:690–9.

Fischl B, Sereno MI, Tootell RBH, *et al.* (1999) High-resolution intersubject averaging and a coordinate system for the cortical surface. *Hum Brain Mapp* **8**:272–84.

Fischl B, Rajendran N, Busa E, *et al.* (2008) Cortical folding patterns and predicting cytoarchitecture. *Cereb Cortex* **18**:1973–80.

Fischl B (2012) FreeSurfer. *Neuroimage* **62**:774–81.

Florio M, Huttner WB (2014) Neural progenitors, neurogenesis and the evolution of the neocortex. *Development* **141**:2182–94.

Fornito A, Yücel M, Wood S, *et al.* (2004) Individual differences in anterior cingulate/paracingulate morphology are related to executive functions in healthy males. *Cereb Cortex* **14**:424–31.

Fox MD, Raichle ME (2007) Spontaneous fluctuations in brain activity observed with functional magnetic resonance imaging. *Nat Rev Neurosci* **8**:700–11.

Friston K (2009) Causal modelling and brain connectivity in functional magnetic resonance imaging. *PLoS Biol* **7**:e1000033.

Friston KJ (2011) Functional and effective connectivity: a review. *Brain Connect* **1**:13–36.

Frost MA, Goebel R (2012) Measuring structural-functional correspondence: spatial variability of specialised brain regions after macro-anatomical alignment. *Neuroimage* **59**:1369–81.

Fulcher BD, Murray JD, Zerbi V, *et al.* (2019) Multimodal gradients across mouse cortex. *Proc Natl Acad Sci USA* **116**:4689–95.

Gao W, Zhu H, Giovanello KS, *et al.* (2009) Evidence on the emergence of the brain's default network from 2-week-old to 2-year-old healthy pediatric subjects. *Proc Natl Acad Sci USA* **106**:6790–5.

Ge F, Li X, Razavi MJ, *et al.* (2018) Denser growing fiber connections induce 3-hinge gyral folding. *Cereb Cortex* **28**:1064–75.

Ge F, Zhang S, Huang H, *et al.* (2019). Exploring intrinsic functional differences of gyri, sulci and 2-hinge, 3-hinge joints on cerebral cortex. In: IEEE 16th International Symposium on Biomedical Imaging (ISBI 2019), IEEE. Venice, Italy; 1585–89 .

Gertz CC, Kriegstein AR (2015) Neuronal migration dynamics in the developing ferret cortex. *J Neurosci* **35**:14307–15.

Gilbert CD, Sigman M (2007) Brain states: top-down influences in sensory processing. *Neuron* **54**:677–96.

Glasser MF, Sotiropoulos SN, Wilson JA, *et al.* (2013) The minimal preprocessing pipelines for the Human Connectome Project. *Neuroimage* **80**:105–24.

Glaunes J, Vaillant M, Miller MI (2004) Landmark matching via large deformation diffeomorphisms on the sphere: special issue on mathematics and image analysis. *J Math Imaging Vision* **20**:179–200.

Goebel R, Esposito F, Formisano E (2006) Analysis of functional image analysis contest (fiac) data with brainvoyager qx: from single-subject to cortically aligned group general linear model analysis and self-organizing group independent component analysis. *Hum Brain Mapp* **27**:392–401.

Goldberg T (2003) Neurocognitive deficits in schizophrenia. *Schizophrenia* 168–84.

Golik P, Tüske Z, Schlüter R, *et al.* (2015) Convolutional neural networks for acoustic modeling of raw time signal in LVCSR. *The 16th Annual Conference of the International Speech Communication Association*. Dresden, Germany; 26–30.

Goualher GL, Barillot C, Bizais Y (1997) Three-dimensional segmentation and representation of cortical sulci using active ribbons. *Int J Pattern Recognit Artif Intell* **11**:1295–315.

Gratiolet P (1854) *Mémoire sur les plis cérébraux de l'homme et des primates*. Vol. **1**. Paris: A. Bertrand.

Gur RC, Moelter ST, Ragland JD (2000) Learning and memory in schizophrenia. In: Sharma T, Harvey P (eds), *Cognition in Schizophrenia : Impairments, Importance, Treatment Strategies*. Oxford: Oxford University Press, 73–91.

Hagemeyer N, Hanft K-M, Akriditou M-A, *et al.* (2017) Microglia contribute to normal myelinogenesis and to oligodendrocyte progenitor maintenance during adulthood. *Acta Neuropathol* **134**:441–58.

Hasnain MK, Fox PT, Woldorff MG (2001) Structure–function spatial covariance in the human visual cortex. *Cereb Cortex* **11**:702–16.

Hansen DV, Lui JH, Parker PRL, *et al.* (2010) Neurogenic radial glia in the outer subventricular zone of human neocortex. *Nature* **464**:554–61.

Hardan AY, Jou RJ, Keshavan MS, *et al.* (2004) Increased frontal cortical folding in autism: a preliminary MRI study. *Psyc Res Neuroimaging* **131**:263–8.

He Y, Chen ZJ, Evans AC (2007) Small-world anatomical networks in the human brain revealed by cortical thickness from MRI. *Cereb Cortex* **17**:2407–19.

Hellier P, Barillot C (2003) Coupling dense and landmark-based approaches for nonrigid registration. *IEEE Trans Med Imaging* **22**:217–27.

Hilgetag CC, Barbas H (2005) Developmental mechanics of the primate cerebral cortex. *Anat Embryol* **210**:411–7.

Hinds OP, Rajendran N, Polimeni JR, *et al.* (2008) Accurate prediction of V1 location from cortical folds in a surface coordinate system. *Neuroimage* **39**:1585–99.

Huang H, Xue R, Zhang J, *et al.* (2009) Anatomical characterization of human fetal brain development with diffusion tensor magnetic resonance imaging. *J Neurosci* **29**:4263–73.

Huang H, Hu X, Zhao Y, *et al.* (2017) Modeling task fMRI data via deep convolutional autoencoder. *IEEE Trans Med Imaging* **37**:1551–61.

Huntenburg JM, Bazin PL, Margulies DS (2018) Large-scale gradients in human cortical organization. *Trends Cogn Sci* **22**:21–31.

Im K, Jo HJ, Mangin JF, *et al.* (2010) Spatial distribution of deep sulcal landmarks and hemispherical asymmetry on the cortical surface. *Cereb Cortex* **20**:602–11.

Im K, Choi YY, Yang JJ, *et al.* (2011) The relationship between the presence of sulcal pits and intelligence in human brains. *Neuroimage* **55**:1490–6.

Jiang M, Yang S, Yan J, *et al.* (2020) Exploring functional difference between gyri and sulci via region-specific 1D convolutional neural networks. *The International Workshop on Machine Learning in Medical Imaging*. Lima, Peru: Springer, 250–9.

Jiang X, Li X, Lv J, *et al.* (2015a) Sparse representation of HCP grayordinate data reveals novel functional architecture of cerebral cortex. *Hum Brain Mapp* **36**:5301–19.

Jiang X, Zhang T, Zhu D, *et al.* (2015b) Anatomy-guided dense individualized and common connectivity-based cortical landmarks (A-DICCCOL). *IEEE Trans Biomed Eng* **62**:1108–19.

Jiang X, Li X, Lv J, *et al.* (2018a) Temporal dynamics assessment of spatial overlap pattern of functional brain networks reveals novel functional architecture of cerebral cortex. *IEEE Trans Biomed Eng* **65**:1183–92.

Jiang X, Zhao L, Liu H, *et al.* (2018b) A cortical folding pattern-guided model of intrinsic functional brain networks in emotion processing. *Front Neurosci* **12**:575.

Johnson HJ, Christensen GE (2002) Consistent landmark and intensity-based image registration. *IEEE Trans Med Imaging* **21**:450–61.

Johnson MB, Wang PP, Atabay KD, *et al.* (2015) Single-cell analysis reveals transcriptional heterogeneity of neural progenitors in human cortex. *Nat Neurosci* **18**:637–46.

Joshi SC, Miller MI (1997) On the geometry and shape of brain sub-manifolds. *Int J Pattern Recognit Artif Intell* **11**:1317–43.

Joshi A, Shattuck D, Thompson P, *et al.* (2007) Surface-constrained volumetric brain registration using harmonic mappings. *IEEE Trans Med Imaging* **26**:1657–69.

Joshi AA, Shattuck DW, Damasio H, *et al.* (2012) Geodesic curvature flow on surfaces for automatic sulcal delineation. *IEEE Int Symp Biomed Imaging (ISBI)* 430–3.

Kaiser M, Hilgetag CC (2006) Nonoptimal component placement, but short processing paths, due to long-distance projections in neural systems. *PLoS Comput Biol* **2**:e95.

Kandel ER, Schwartz JH, Jessell TM (2000) *Principles of Neural Science*, 4th edn, **50**. McGraw-Hill, 823–39.

Kao CY, Hofer M, Sapiro G, *et al.* (2007) A geometric method for automatic extraction of sulcal fundi. *IEEE Trans Med Imaging* **26**:530–40.

Kikinis R, Shenton ME, Gerig G, *et al.* (1994) Temporal lobe sulco-gyral pattern anomalies in schizophrenia: an in vivo MR three-dimensional surface rendering study. *Neurosci Lett* **182**:7–12.

Krienen FM, Yeo BT, Ge T, *et al.* (2016) Transcriptional profiles of supragranular-enriched genes associate with corticocortical network architecture in the human brain. *Proc Natl Acad Sci USA* **113**:E469–78.

Kroenke CD, Bayly PV (2018) How forces fold the cerebral cortex. *J Neurosci* **38**:767–75.

Laughlin SB, Sejnowski TJ (2003) Communication in neuronal networks. *Science* **301**:1870–4.

LeCun Y, Bengio Y, Hinton G (2015) Deep learning. *Nature* **521**:436–44.

Levitt JG, Blanton RE, Smalley S, *et al.* (2003) Cortical sulcal maps in autism. *Cereb Cortex* **13**:728–35.

Lewitus E, Kelava I, Kalinka AT, *et al.* (2014) An adaptive threshold in mammalian neocortical evolution. *PLoS Biol* **12**:e1002000.

Li G, Guo L, Nie J, *et al.* (2009) Automatic cortical sulcal parcellation based on surface principal direction flow field tracking. *Neuroimage* **46**:923–37.

Li G, Guo L, Nie J, *et al.* (2010) An automated pipeline for cortical sulcal fundi extraction. *Med Image Anal* **14**:343–59.

Li K, Guo L, Li G, *et al.* (2010) Gyral folding pattern analysis via surface profiling. *Neuroimage* **52**:1202–14.

Li X, Hu X, Jiang X, *et al.* (2013) Assessing structural organization and functional interaction in gyral, sulcal and cortical networks. *The International Workshop on Multimodal Brain Image Analysis* **8159**:9–17.

Li X, Zhu D, Jiang X, *et al.* (2014) Dynamic functional connectomics signatures for characterization and differentiation of PTSD patients. *Hum Brain Mapp* **35**:1761–78.

Li X, Chen H, Zhang T, *et al.* (2017) Commonly preserved and species-specific gyral folding patterns across primate brains. *Brain Struct Funct* **222**:2127–41.

Li X, Liu T, Liu Y, *et al.* (2020a) Marmoset brain ISH data revealed molecular difference between cortical folding patterns. *Cereb Cortex* **31**:1660–74.

Li Y, Sescousse G, Amiez C, *et al.* (2015) Local morphology predicts functional organization of experienced value signals in the human orbitofrontal cortex. *J Neurosci* **35**:1648–58.

Li Y, Huang H, Chen H, *et al.* (2020b) Deep neural networks for in situ hybridization grid completion and clustering. *IEEE/ACM Trans Comput Biol Bioinf* **17**:536–46.

Litjens G, Kooi T, Bejnordi BE, *et al.* (2017) A survey on deep learning in medical image analysis. *Med Image Anal* **42**:60–88.

Liu H, Jiang X, Zhang T, *et al.* (2017) Elucidating functional differences between cortical gyri and sulci via sparse representation HCP grayordinate fMRI data. *Brain Res* **1672**:81–90.

Liu H, Zhang S, Jiang X, *et al.* (2019) The cerebral cortex is bisectionally segregated into two fundamentally different functional units of gyri and sulci. *Cereb Cortex* **29**:4238–52.

Logothetis NK (2008) What we can do and what we cannot do with fMRI. *Nature* **453**:869–78.

Lohmann G (1998) Extracting line representations of sulcal and gyral patterns in MR images of the human brain. *IEEE Trans Med Imaging* **17**:1040–8.

Lohmann G, von Cramon DY (2000) Automatic labelling of the human cortical surface using sulcal basins. *Med Image Anal* **4**:179–88.

Lohmann G, von Cramon DY, Colchester AC (2008) Deep sulcal landmarks provide an organizing framework for human cortical folding. *Cereb Cortex* **18**:1415–20.

Lopez-Persem A, Verhagen L, Amiez C, *et al.* (2019) The human ventromedial prefrontal cortex: sulcal morphology and its influence on functional organization. *J Neurosci* **39**:3627–39.

Lv J, Jiang X, Li X, *et al.* (2014) Holistic atlases of functional networks and interactions reveal reciprocal organizational

architecture of cortical function. *IEEE Trans Biomed Eng* **62**:1120–31.

Lv J, Jiang X, Li X, *et al.* (2015) Sparse representation of whole-brain fMRI signals for identification of functional networks. *Med Image Anal* **20**:112–34.

Mairal J, Bach F, Ponce J, *et al.* (2010) Online learning for matrix factorization and sparse coding. *J Machine Learn Res* **11**:19–60.

Mallat SG (1989) A theory for multiresolution signal decomposition: the wavelet representation. *IEEE Trans Pattern Anal Mach Intell* **11**:674–93.

Mangin JF, Frouin V, Bloch I, *et al.* (1995) From 3D magnetic resonance images to structural representations of the cortex topography using topology preserving deformations. *J Math Imaging Vis* **5**:297–318.

Mangin JF, Le Guen Y, Labra N, *et al.* (2019) "*Plis de passage*" deserve a role in models of the cortical folding process. *Brain Topogr* **32**:1035–48.

Meinhardt H, Gierer A (1974) Applications of a theory of biological pattern formation based on lateral inhibition. *J Cell Sci* **15**:321–46.

Meng Y, Li G, Lin W, *et al.* (2014) Spatial distribution and longitudinal development of deep cortical sulcal landmarks in infants. *Neuroimage* **100**:206–18.

Mikula S, Trotts I, Stone J, *et al.* (2007) Internet-enabled high-resolution brain mapping and virtual microscopy. *Neuroimage* **35**:9–15.

Miller JA, Ding S-L, Sunkin SM, *et al.* (2014) Transcriptional landscape of the prenatal human brain. *Nature* **508**:199–206.

Morosan P, Rademacher J, Schleicher A, *et al.* (2001) Human primary auditory cortex: cytoarchitectonic subdivisions and mapping into a spatial reference system. *Neuroimage* **13**:684–701.

Nakamasu A, Takahashi G, Kanbe A, *et al.* (2009) Interactions between zebrafish pigment cells responsible for the generation of Turing patterns. *Proc Natl Acad Sci USA* **106**:8429–34.

Nakamura M, Nestor PG, McCarley RW, *et al.* (2007) Altered orbitofrontal sulcogyral pattern in schizophrenia. *Brain* **130**:693–707.

Nakamura M, Nestor PG, Shenton ME (2020) Orbitofrontal sulcogyral pattern as a transdiagnostic trait marker of early neurodevelopment in the social brain. *Clin EEG Neurosci* **51**:1550059420904180.

Narr KL, Bilder RM, Kim S, *et al.* (2004) Abnormal gyral complexity in first-episode schizophrenia. *Biol Psychiatry* **55**:859–67.

Nie J, Guo L, Li K, *et al.* (2012) Axonal fiber terminations concentrate on gyri. *Cereb Cortex* **22**:2831–9.

Noctor SC, Martínez-Cerdeño V, Ivic L, *et al.* (2004) Cortical neurons arise in symmetric and asymmetric division zones and migrate through specific phases. *Nat Neurosci* **7**:136–44.

Nordahl CW, Dierker D, Mostafavi I, *et al.* (2007) Cortical folding abnormalities in autism revealed by surface-based morphometry. *J Neurosci* **27**:11725–35.

Öngür D, Price JL (2000) The organization of networks within the orbital and medial prefrontal cortex of rats, monkeys and humans. *Cereb Cortex* **10**:206–19.

Ono M, Kubick S, Abernathey C (1990) *Atlas of the Cerebral Sulci.* Thieme Medical Publishers.

Orban GA, Van Essen D, Vanduffel W (2004) Comparative mapping of higher visual areas in monkeys and humans. *Trends Cogn Sci* **8**:315–24.

Ou J, Lian Z, Xie L, *et al.* (2014) Atomic dynamic functional interaction patterns for characterization of ADHD. *Hum Brain Mapp* **35**:5262–78.

Ouyang M, Kang H, Detre JA, *et al.* (2017) Short-range connections in the developmental connectome during typical and atypical brain maturation. *Neurosci Biobehav Rev* **83**:109–22.

Pantazis D, Joshi A, Jiang J, *et al.* (2010) Comparison of landmark-based and automatic methods for cortical surface registration. *Neuroimage* **49**:2479–93.

Parent A (2014) Louis Pierre Gratiolet (1815-1865) and his contribution to the study of cerebral convolutions in primates. *Neurosci Med* **5**:1–8.

Patti MA, Troiani V (2018) Orbitofrontal sulcogyral morphology is a transdiagnostic indicator of brain dysfunction. *NeuroImage: Clinical* **17**:910–7.

Penttonen M, Buzsáki G (2003) Natural logarithmic relationship between brain oscillators. *Thalamus Related Systems* **2**:145–52.

Pilz G-A, Shitamukai A, Reillo I, *et al.* (2013) Amplification of progenitors in the mammalian telencephalon includes a new radial glial cell type. *Nat Commun* **4**:2125.

Piven J, Berthier ML, Starkstein SE, *et al.* (1990) Magnetic resonance imaging evidence for a defect of cerebral cortical development in autism. *Am J Psychiatry* **147**:734–9.

Rakic P (1988) Specification of cerebral cortical areas. *Science* **241**:170–6.

Rash BG, Duque A, Morozov YM, *et al.* (2019) Gliogenesis in the outer subventricular zone promotes enlargement and gyrification of the primate cerebrum. *Proc Natl Acad Sci USA* **116**:7089–94.

Razavi MJ, Zhang T, Li X, *et al.* (2015) Role of mechanical factors in cortical folding development. *Phys Rev E* **92**:032701.

Régis J, Mangin J-F, Ochiai T, *et al.* (2005) "Sulcal root" generic model: a hypothesis to overcome the variability of the human cortex folding patterns. *Neurol. Med. Chir.* **45**:1–17.

Reillo I, de Juan Romero C, García-Cabezas MÁ, *et al.* (2011) A role for intermediate radial glia in the tangential expansion of the mammalian cerebral cortex. *Cereb Cortex* **21**:1674–94.

Reillo I, Borrell V (2012) Germinal zones in the developing cerebral cortex of ferret: ontogeny, cell cycle kinetics, and diversity of progenitors. *Cereb Cortex* **22**:2039–54.

Rettmann ME, Han X, Xu C, *et al.* (2002) Automated sulcal segmentation using watersheds on the cortical surface. *Neuroimage* **15**:329–44.

Reveley C, Seth AK, Pierpaoli C, *et al.* (2015) Superficial white matter fiber systems impede detection of long-range cortical connections in diffusion MR tractography. *Proc Natl Acad Sci USA* **112**:E2820–8.

Richiardi J, Altmann A, Milazzo AC, *et al.* (2015) Correlated gene expression supports synchronous activity in brain networks. *Science* **348**:1241–4.

Richman DP, Stewart R, Caviness V, Jr (1974) Cerebral microgyria in a 27-week fetus: an architectonic and topographic analysis. *J Neuropathol Exp Neurol* **33**:374–84.

Richman DP, Stewart RM, Hutchinson JW, Jr (1975) Mechanical model of brain convolutional development. *Science* **189**:18–21.

Rilling JK, Glasser MF, Preuss TM, *et al.* (2008) The evolution of the arcuate fasciculus revealed with comparative DTI. *Nat Neurosci* **11**:426–8.

Rivière D, Mangin JF, Papadopoulos-Orfanos D, *et al.* (2002) Automatic recognition of cortical sulci of the human brain using a congregation of neural networks. *Med Image Anal* **6**:77–92.

Roland PE, Zilles K (1994) Brain atlases - a new research tool. *Trends Neurosci* **17**:458–67.

Roland PE, Zilles K (1998) Structural divisions and functional fields in the human cerebral cortex. *Brain Res Rev* **26**:87–105.

Ronan L, Voets N, Rua C, *et al.* (2014) Differential tangential expansion as a mechanism for cortical gyrification. *Cereb Cortex* **24**:2219–28.

Roth G, Dicke U (2005) Evolution of the brain and intelligence. *Trends Cogn Sci* **9**: 250–7.

Rubinov M, Sporns O (2010) Complex network measures of brain connectivity: uses and interpretations. *Neuroimage* **52**:1059–69.

Sang Y-F, Wang D, Wu J-C, *et al.* (2011) Wavelet-based analysis on the complexity of hydrologic series data under multi-temporal scales. *Entropy* **13**:195–210.

Sepulcre J, Liu H, Talukdar T, *et al.* (2010) The organization of local and distant functional connectivity in the human brain. *PLoS Comput Biol* **6**:e1000808.

Shen D, Davatzikos C (2003) Very high-resolution morphometry using mass-preserving deformations and hammer elastic registration. *Neuroimage* **18**:28–41.

Shen D, Wu G, Suk HI (2017) Deep learning in medical image analysis. *Annu Rev Biomed Eng* **19**:221–48.

Shenton ME, Dickey CC, Frumin M, *et al.* (2001) A review of MRI findings in schizophrenia. *Schizophr Res* **49**:1–52.

Siegel M, Donner TH, Engel AK (2012) Spectral fingerprints of large-scale neuronal interactions. *Nat Rev Neurosci* **13**:121–34.

Smart IHM, Dehay C, Giroud P, *et al.* (2002) Unique morphological features of the proliferative zones and postmitotic compartments of the neural epithelium giving rise to striate and extrastriate cortex in the monkey. *Cereb Cortex* **12**: 37–53.

Smith SM, Fox PT, Miller KL, *et al.* (2009) Correspondence of the brain's functional architecture during activation and rest. *Proc Natl Acad Sci* **106**:13040–5.

Smith SM, Miller KL, Salimi-Khorshidi G, *et al.* (2011) Network modelling methods for FMRI. *Neuroimage* **54**:875–91.

Smith SM, Beckmann CF, Andersson J, *et al.* (2013) Resting-state fMRI in the human connectome project. *Neuroimage* **80**:144–68.

Stahl R, Walcher T, De Juan Romero C, *et al.* (2013) TRNP1 regulates expansion and folding of the mammalian cerebral cortex by control of radial glial fate. *Cell* **153**:535–49.

Stutterd CA, Leventer RJ (2014) Polymicrogyria: a common and heterogeneous malformation of cortical development. *Am J Med Genet* **166C**:227–39.

Takahashi E, Dai G, Wang R, *et al.* (2010) Development of cerebral fiber pathways in cats revealed by diffusion spectrum imaging. *Neuroimage* **49**:1231–40.

Takahashi E, Folkerth RD, Galaburda AM, *et al.* (2012) Emerging cerebral connectivity in the human fetal brain: an MR tractography study. *Cereb Cortex* **22**:455–64.

Talairach J, Szikla G (1967) *Atlas of Stereotaxic Anatomy of the Telencephalon*. Paris: Masson and Cie.

Taverna E, Götz M, Huttner WB (2014) The cell biology of neurogenesis: toward an understanding of the development and evolution of the neocortex. *Annu Rev Cell Dev Biol* **30**: 465–502.

Thompson PM, Toga AW (1996) A surface-based technique for warping three dimensional images of the brain. *IEEE Trans Med Imaging* **15**:402–17.

Thompson PM, Woods RP, Mega M, *et al.* (2000) Mathematical/computational challenges in creating deformable and probabilistic atlases of the human brain. *Hum Brain Mapp* **9**:81–92.

Toro R, Burnod Y (2003) Geometric atlas: modeling the cortex as an organized surface. *Neuroimage* **20**:1468–84.

Tosun D, Rettmann ME, Prince JL (2004) Mapping techniques for aligning sulci across multiple brains. *Med Image Anal* **8**:295–309.

Troiani V, Patti MA, Adamson K (2020) The use of the orbitofrontal H-sulcus as a reference frame for value signals. *Eur J Neurosci* **51**:1928–43.

Turing AM (1952) The chemical basis of morphogenesis. *Philosoph Transac R Soc of Lond Series B, Biol Sci* **237**:37–72.

Tzourio-Mazoyer N, Landeau B, Papathanassiou D, *et al.* (2002) Automated anatomical labeling of activations in SPM using a macroscopic anatomical parcellation of the MNI MRI single-subject brain. *Neuroimage* **15**:273–89.

Uddin LQ, Supekar K, Amin H, *et al.* (2010) Dissociable connectivity within human angular gyrus and intraparietal sulcus: evidence from functional and structural connectivity. *Cereb Cortex* **20**:2636–46.

Van Den Heuvel MP, Sporns O (2011) Rich-club organization of the human connectome. *J Neurosci* **31**:15775–86.

Van Den Heuvel MP, Kahn RS, Goñi J, *et al.* (2012) High-cost, high-capacity backbone for global brain communication. *Proc Natl Acad Sci USA* **109**:11372–7.

Van Essen DC (1997) A tension-based theory of morphogenesis and compact wiring in the central nervous system. *Nature* **385**:313–8.

Van Essen DC, Drury HA, Joshi S, *et al.* (1998) Functional and structural mapping of human cerebral cortex: solutions are in the surfaces. *Proc Natl Acad Sci USA* **95**:788–95.

Van Essen DC (2005) A population-average, landmark- and surface-based (pals) atlas of human cerebral cortex. *Neuroimage* **28**:635–62.

Van Essen DC, Smith SM, Barch DM, *et al.* (2013) The WU-Minn human connectome project: an overview. *Neuroimage* **80**: 62–79.

Von Stein A, Sarnthein J (2000) Different frequencies for different scales of cortical integration: from local gamma to long range alpha/theta synchronization. *Int J Psychophysiol* **38**:301–13.

Wang X, Tsai JW, LaMonica B, *et al.* (2011) A new subtype of progenitor cell in the mouse embryonic neocortex. *Nat Neurosci* **14**:555–61.

Watanabe H, Nakamura M, Ohno T, *et al.* (2014) Altered orbitofrontal sulcogyral patterns in adult males with high-functioning autism spectrum disorders. *Soc Cogn Affect Neurosci* **9**:520–8.

Watson JDG, Myers R, Frackowiak RSJ, *et al.* (1993) Area v5 of the human brain: evidence from a combined study using positron emission tomography and magnetic resonance imaging. *Cereb Cortex* **3**:79–94.

Watts DJ, Strogatz SH (1998) Collective dynamics of 'small-world' networks. *Nature* **393**:440–2.

Weiner KS, Natu VS, Grill-Spector K (2018) On object selectivity and the anatomy of the human fusiform gyrus. *Neuroimage* **173**:604–9.

White T, Andreasen NC, Nopoulos P, *et al.* (2003) Gyrification abnormalities in childhood-and adolescent-onset schizophrenia. *Biol Psychiatry* **54**:418–26.

White T, Su S, Schmidt M, *et al.* (2010) The development of gyrification in childhood and adolescence. *Brain Cogn* **72**: 36–45.

Whittle S, Allen NB, Fornito A, *et al.* (2009) Variations in cortical folding patterns are related to individual differences in temperament. *Psychiatry Research: Neuroimaging* **172**:68–74.

Wing L (1997) The autistic spectrum. *Lancet North Am Ed* **350**:1761–6.

Woods R, Grafton ST, Holmes CJ, *et al.* (1998) Automated image registration: I. general methods and intrasubject, intramodality validation. *J Comput Assist Tomogr* **22**: 139–52.

Xu G, Knutsen AK, Dikranian K, *et al.* (2010) Axons pull on the brain, but tension does not drive cortical folding. *J Biomech Eng* **132**:071013.

Yagi A (2009) *Abstract Parabolic Evolution Equations and their Applications*. Springer Berlin Heidelberg.

Yang S, Zhao Z, Cui H, *et al.* (2019) Temporal variability of cortical gyral-sulcal resting state functional activity correlates with fluid intelligence. *Front Neural Circ* **13**:36.

Yoshino M, Saito K, Kawasaki K, *et al.* (2020) The origin and development of subcortical U-fibers in gyrencephalic ferrets. *Mol Brain* **13**:1–9.

Yu X, Chen H, Zhang T, *et al.* (2013) Joint analysis of gyral folding and fiber shape patterns. In: *The 2013 IEEE 10th International Symposium on Biomedical Imaging*.

Yuan J, Li X, Zhang J, *et al.* (2018) Spatio-temporal modeling of connectome-scale brain network interactions via time-evolving graphs. *Neuroimage* **180**:350–69.

Zeng T, Chen H, Fakhry A, *et al.* (2015) Allen mouse brain atlases reveal different neural connection and gene expression patterns in cerebellum gyri and sulci. *Brain Struct Funct* **220**:2691–703.

Zhang D, Guo L, Zhu D, *et al.* (2013) Diffusion tensor imaging reveals evolution of primate brain architectures. *Brain Struct Funct* **218**:1429–50.

Zhang S, Liu H, Huang H, *et al.* (2018) Deep learning models unveiled functional difference between cortical gyri and sulci. *IEEE Trans Biomed Eng* **66**:1297–308.

Zhang S, Zhao Y, Jiang X, *et al.* (2018b) Joint representation of consistent structural and functional profiles for identification of common cortical landmarks. *Brain Imaging Behav* **12**: 728–42.

Zhang S, Dong Q, Zhang W, *et al.* (2019a) Discovering hierarchical common brain networks via multimodal deep belief network. *Med Image Anal* **54**:238–52.

Zhang S, Jiang X, Zhang W, *et al.* (2019b) Joint representation of connectome-scale structural and functional profiles for identification of consistent cortical landmarks in macaque brain. *Brain Imaging Behav* **13**:1427–43.

Zhang T, Chen H, Guo L, *et al.* (2014) Characterization of U-shape streamline fibers: methods and applications. *Med Image Anal* **18**:795–807.

Zhang T, Razavi MJ, Li X, *et al.* (2016) Mechanism of consistent gyrus formation: an experimental and computational study. *Sci Rep* **6**:1–11.

Zhang T, Razavi MJ, Chen H, *et al.* (2017) Mechanisms of circumferential gyral convolution in primate brains. *J Comput Neurosci* **42**:217–29.

Zhang T, Li X, Jiang X, *et al.* (2020) Cortical 3-hinges could serve as hubs in cortico-cortical connective network. *Brain Imaging Behav* 1–18.

Zhang W, Lv J, Li X, *et al.* (2019) Experimental comparisons of sparse dictionary learning and independent component analysis for brain network inference from fMRI data. *IEEE Trans Biomed Eng* **66**:289–99.

Zhao L, Zhang T, Guo L, *et al.* (2020) Gyral-sulcal contrast in intrinsic functional brain networks across task performances. *Brain Imaging Behav* **3**:1–16.

Zhou B, Khosla A, Lapedriza A, *et al.* (2016) *Learning deep features for discriminative localization*. In: The Proceedings of the IEEE Conference on Computer Vision and Pattern Recognition. Las Vegas, NV, USA: IEEE , 2921–9 .

Zhou Y, Thompson PM, Toga AW (1999) Extracting and representing the cortical sulci. *IEEE Comput Graph Appl* **19**: 49–55.

Zhu D, Li K, Guo L, *et al.* (2013) DICCCOL: dense individualized and common connectivity-based cortical landmarks. *Cereb Cortex* **23**:786–800.

Zilles K, Schleicher A, Langemann C, *et al.* (1997) Quantitative analysis of sulci in the human cerebral cortex: development, regional heterogeneity, gender difference, asymmetry, intersubject variability and cortical architecture. *Hum Brain Mapp* **5**:218–22.